A VORTICITY-BASED ANALYSIS OF THE SPATIAL AND TEMPORAL CHARACTERISTICS OF THE BEAUFORT ANTICYCLONE

BY

KIRSTIN JOY GLEICHER

THESIS

Submitted in partial fulfillment of the requirements
for the degree of Master of Science in Atmospheric Sciences
in the Graduate College of the
University of Illinois at Urbana-Champaign, 2010

Urbana, Illinois

Adviser:

Professor Emeritus John E. Walsh

Abstract

The Beaufort Anticyclone is the dominate pressure feature over the Arctic Ocean in all seasons and has a large influence on the surface wind regime and sea-ice motion. Sea level pressure (SLP) from the NCAR/NCEP Reanalysis is used to create a vorticity metric to investigate the spatial and temporal characteristics of the Beaufort Anticyclone from 1948-2008. Vorticity averaged over the Beaufort Anticyclone region correlated with Northern Hemisphere SLP show areas of strongest relationship south of Alaska and north of Siberia. These two areas are also present in SLP composite maps created using the vorticity timeseries. The spatial characteristics are investigated further by creating a timeseries of rapid change events. SLP maps of these events reveal similar features south of Alaska and north of Siberia. Temporal characteristics are investigated using running means and spectral analysis, which show an annual cycle.

Teleconnection patterns have been shown to have an influence over the Arctic. The Beaufort Anticyclone vorticity metric is correlated with teleconnection index values; the Pacific Ocean patterns show a larger influence than the Atlantic patterns, contrary to past studies that show the Arctic Oscillation as a main driver over the Arctic. A significant correlation is found with the Pacific North American pattern in all seasons except summer. The El Niño Southern Oscillation shows a significant correlation in winter, and the Pacific Decadal Oscillation shows a significant correlation in winter and spring.

To Mom and Dad

Acknowledgments

National Science Foundation grant number ARC-0732650 for funding this research project. Many thanks to the following people for their contributions to my project: John for being a patient and encouraging adviser and giving me the opportunity to explore my research interests. Bill for spending all those hours trying to teach me how to program, I wouldn't have any results without you! Dan for being there to calm me down when I hit bumps in the road. Oscar, Chase, and Maresha for providing the cuddle support as needed. Dad for all the advice on life, I wouldn't have made it here without you. And most importantly, my mom for encouraging me to follow my interests and letting me stand outside in thunderstorms when I was little!

Table of Contents

1. Introduction

The general circulation of the atmosphere is a topic learned at the beginning of every atmospheric scientist's education. It is from this introductory knowledge that scientists learn about subsidence and high pressure over the Polar Regions. Figure 1.1 is an introductory figure showing the general circulation of the atmosphere with the basic zonal wind structure and high pressure at the poles. Of course this figure is only an ideological schematic of the atmospheric circulation and as a scientist begins to look from theory to reality, the polar high pressure feature still remains. Figure 1.2 shows the Northern Hemisphere average sea level pressure (SLP) pattern for winter (a) and summer (b). In both seasons, a high pressure center can be seen in the vicinity of the North Pole. It is the robustness of this high latitude anticyclone this study wishes to investigate.

Located over the Beaufort Sea, north of Alaska, the Beaufort Anticyclone is the dominate pressure feature. It is an extremely important feature in Arctic dynamics because it dictates the surface wind pattern and ultimately sea ice transport in the Arctic Ocean (Coon et al., 1974). Figure 1.3 depicts sea ice motion over the Arctic Ocean. There is a large clockwise circulation over the Beaufort Sea showing the Beaufort Anticyclone's influence on surface sea ice motion. Though this feature has been mentioned in studies as early as the 1950s and 1960s (Prik, 1959, Reed and Kunkel 1960), there have been few studies that focus on the Beaufort Anticyclone's temporal variability and its interactions with the climate system.

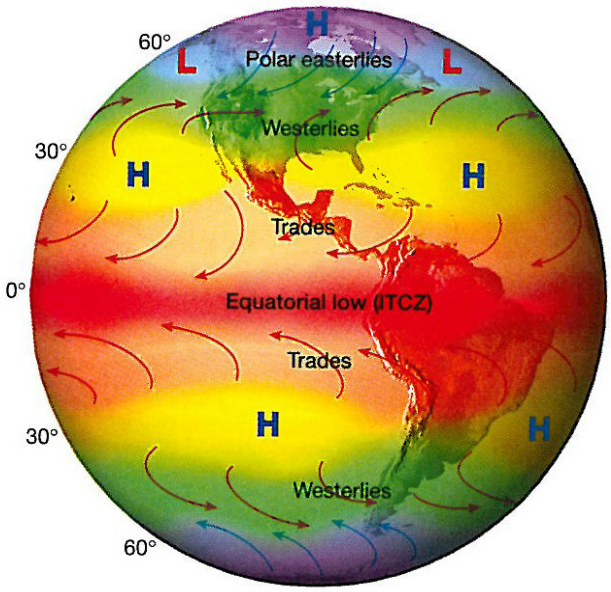

Figure 1.1: Basic zonal wind structure showing semipermanent high and low pressure patterns (from Lutgens and Tarbuck, 2001)

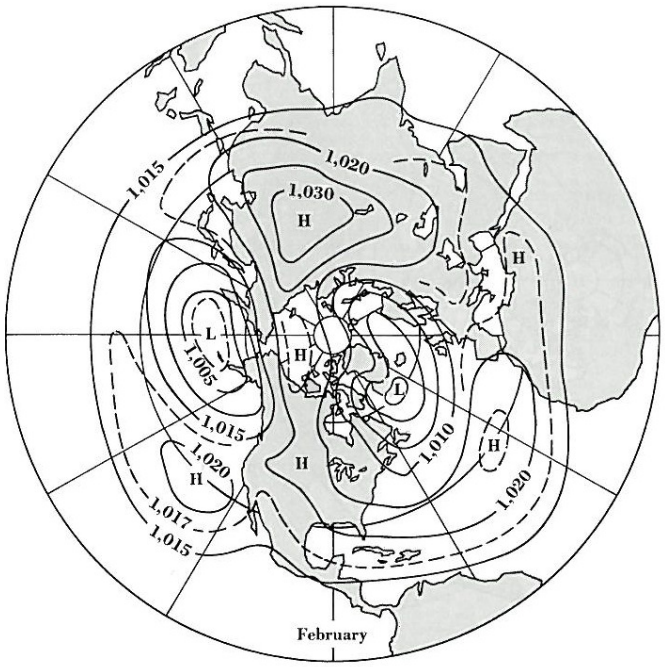

Figure 1.2(a): Average sea level pressures for the northern hemisphere in winter (from Petterssen, 1969)

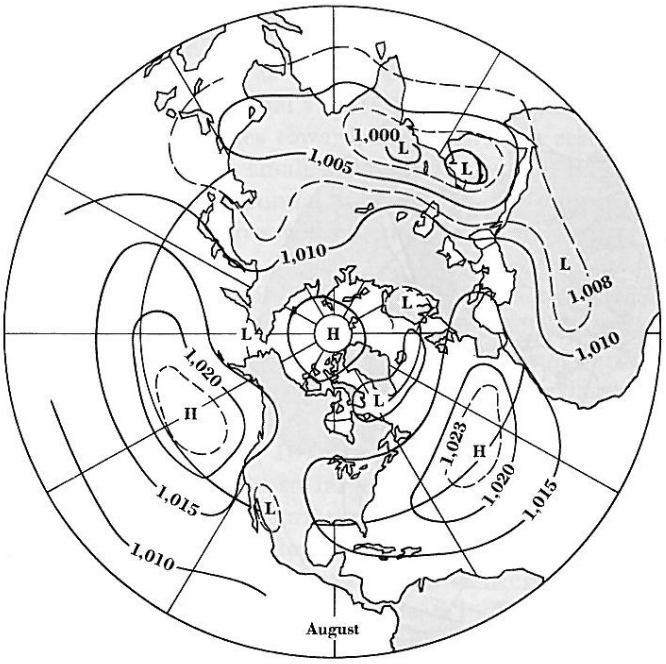

Figure 1.2(b): Same as (a) but for summer

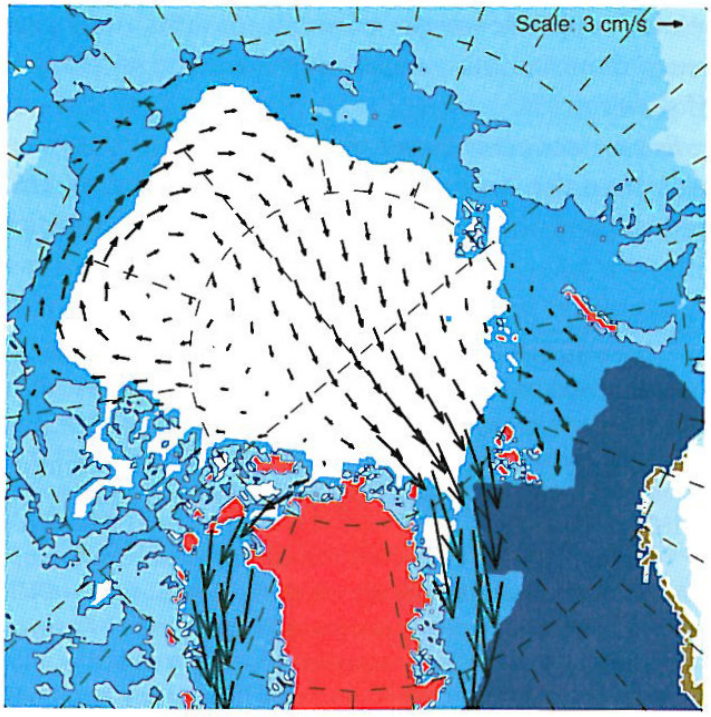

Figure 1.3: Wintertime Arctic sea ice motion as inferred from buoy tracks depicts clockwise motion over Beaufort Sea (from Wallace and Hobbs, 2006)

Early synoptic assessments of the Arctic show the presence of the Beaufort Anticyclone, but a lack of consistent measurements provided a different range of depictions. In a study based on the time period 1952-1956, Reed and Kunkel, 1960, found a closed 1005mb low pressure center over the Arctic in July, whereas a study published by Prik, 1959, show a 1013mb high pressure center north of Alaska. Furthermore, a 12 year study by O'Conner, 1961, states a high pressure center shows up over the Arctic Ocean in January, July, and August, but fails to mention a magnitude. And lastly, Crutcher and Meserve, 1970, show a closed anticyclone in July between the Alaskan coast and North Pole. These early studies only mention the presence of the feature, but do not go into any details about seasonal cycle or interannual variability.

The first study to truly focus on the circulations over the Arctic is Walsh, 1978. Using SLP data for the period 1952-1975, a seasonal cycle and frequency spectrum are created for the region north of 60°N. The seasonal cycle shows closed high pressure centers over the Arctic Ocean during the spring (March-May) and autumn (September-November), a pressure ridge during winter (December-February), and weak gradients over the entire Arctic in summer (June-August). A monthly mean timeseries of pressure averaged over 70°N shows a semiannual oscillation with pressure maxima in spring and autumn.

1979 was a breakthrough year in observations over the Arctic due to the Arctic Ocean Buoy Project (AOBP) (Thorndike and Colony, 1980). Prior to the start of the AOBP, the only pressure measurements over the Arctic Ocean were from occasional drifting ice stations. There were usually only one or two of these stations at a time from

the 1950s through the 1970s, and essentially no observations before about 1950. Due to the absence of observations, analysts in the early 20th century often had a high pressure bias over the Arctic Ocean due to the notion that Polar Regions were dominated by high pressure (Serreze and Barry, 2005).

The AOBP created an improved method for measuring SLP and was the basis for the synoptic assessment paper by Serreze and Barry, 1988. Using the 1979-1985 time period, they show that winter anticyclones are dominate on the Canadian side of the Arctic, including the Beaufort Sea, with similar patterns in spring. Summer and autumn anticyclone patterns show no distinct anticyclone activity over the Beaufort area. In an updated synoptic activity paper by Serreze et al, 1993, the 1952-1989 period was used and winter anticyclones were found to be most common over eastern Siberia, Alaska, and the broad Arctic Ocean region in between. These anticyclone centers tended to disappear during summer except over the Beaufort Sea, where the anticyclone persisted and overlapped with cyclone activity. Another conclusion from this study was the peak strength of the Beaufort Gyre ice circulation in spring is related to the seasonal shift toward stronger anticyclonic activity over the Beaufort Sea and weaker activity over Alaska and Siberia. In looking at these studies, it is important to note that the synoptic patterns over the Arctic Ocean are weaker in summer than other seasons.

Following these synoptic activity papers, there were a few studies published with a new hypothesis about how mass transports across the Arctic and also how the Beaufort Anticyclone builds and decays. Honda et al, 2001, introduces a ‘seesaw’ theory where mass is transferred between the Aleutian and Icelandic low centers over

the Arctic Ocean. Cullather and Lynch, 2003, took this theory and applied it to the annual cycle of SLP over the Arctic. They state that there is an asymmetry to the mass flux during the annual cycle. In spring, they show that mass travels from the Eastern Hemisphere into the Western Hemisphere via the Arctic Basin and vise versa in autumn. As this mass transfer occurs, there is a build up of mass over the Arctic Ocean leading to a strengthening of the Beaufort Anticyclone. This hypothesis is consistent with the Walsh 1978 monthly mean timeseries showing two pressure peaks in spring and autumn over the Arctic.

Looking at the strength of the Beaufort Anticyclone, Proshutinsky and Johnson, 1997, introduce the idea that the SLP over the Arctic Ocean oscillates between an anticyclonic and cyclonic wind regime on a 5-7 year timescale. They found that modeling sea level and ice motion as a proxy for SLP, the wind driven motions are forced by a change of intensity of the Icelandic Low and Siberian High. Rigor et al, 2002, performed another study looking at cyclonic sea ice motion over the arctic. They suggest that atmospheric teleconnections have a role in determining SLP over the Arctic and thus a role in sea ice motion, by stating that if the Arctic Oscillation (AO) shifts toward a positive phase in winter, the Beaufort Anticyclone center shifts to the south creating a more cyclonic area of sea ice motion.

Rigor et al 2002 is one of many papers about teleconnection influences of SLP and sea ice motion, especially with regard to the summer sea ice extent anomalies seen in the recent past. The summer of 2007 had an extreme loss in sea ice, and has prompted many theories as to what caused it. L'Heureux et al., 2008, show the importance of the Pacific-North American (PNA) pattern in the sea ice decline. The

PNA in its positive phase shows anomalous anticyclonic circulations over the Beaufort Sea. In 2007, the PNA index was three standard deviations above the mean, showing an extremely anomalous signal over the Beaufort region. The increase in anticyclonic activity during the summer and winter has been shown to account for 50% of the September sea ice extent (Ogi et al, 2010).

Another study, Wang et al, 2009, shows the Dipole Anomaly (DA) as a major driver to record lows in sea ice extent. The DA is defined as the second empirical orthogonal function of the Arctic SLP fields. Wang et al state that during years of extreme summer sea ice loss, the DA produced a strong meridional wind anomaly toward the Atlantic and enhanced the oceanic heat flux and amplified the ice-albedo feedback.

In looking at the Beaufort Anticyclone's climate interactions, it is important to understand the Arctic's connections to mid/lower latitudes. Wallace and Gutzler, 1980, outline the PNA pattern as a north-south SLP seesaw in the Pacific and present statistics showing negative correlations between the Polar Regions and mid-latitudes. In a recent study, Serreze and Barrett, 2010, the Beaufort Anticyclone is a center of action in many teleconnection patterns including the PNA, AO, DA, and Pacific Decal Oscillation, and is a significant SLP feature through all seasons.

This study seeks to expand knowledge on the Beaufort Anticyclone's temporal variability and spatial associations by looking at the feature from a vorticity framework instead of the traditional SLP. Also, by looking at both temporal and spatial correlations of the anticyclone, there will be a more complete understanding of the feature with respect to mass transport and teleconnection influences. Finally, this

study will try to eliminate the dependence on monthly data for monthly/seasonal timescale features by using a 30 day running mean framework.

2. Data

This section describes the various data sources used to produce results for this study. The methods and results found using each data source are described in more detail in section 3.

2.1 NCEP/NCAR Reanalysis

The NCEP/NCAR Reanalysis (Kalnay, et al., 1996) is the main data source for this project. Because this project relies heavily on the reanalysis, a summary of the generation and comments on both the advantages and disadvantages of the use of a reanalysis are provided in this section.

A reanalysis has the goal of assimilating data from many sources to create a consistent data record using the same analysis scheme. More specifically, the NCEP/NCAR Reanalysis is a joint project between NCEP and NCAR with the goal of producing atmospheric analyses using historical data from 1948 onwards, as well as to produce analyses of the current atmospheric state.

The creation of reanalysis output is completed in three major modules: the first is data decoding and quality control. This task requires the collection and preparation of both surface and upper-air observations. Next the data must go through preprocessing to reformat from the many different data sources to a single format. The preprocessing includes a quality-control process, which allows for detection of major data problems and minimizes the need for reanalysis reruns due to data error. Once the data is preprocessed, the main module of data assimilation can occur. Using a global spectral model and a spectral statistical interpolation analysis scheme, the data

is assimilated and provides gridded output in four classes. Class A is an analysis variable strongly influenced by observations, class B indicates both an observational and model component to the variable, class C indicates a variable solely derived from the model, and class D represents a field obtained from climatological values with no influence from the model. Output from the reanalysis runs from 1948 to present and has a global spatial resolution of 2.5° with temporal scales of 6 hourly averages, daily averages, monthly averages, and other long term means.

Kistler et al, 2001, presents various problems with the NCAR/NCEP reanalysis dataset. The first relates to snow cover during the 1974-1994 time period: snow cover corresponding to 1973 was used for every year by mistake. This error impacts surface regions that were snow free when 1973 had snow cover and has minimal probability for contamination to this study due to the use of SLP only. The second major problem is with the 'paid observation' (PAOB) estimates of SLP. The PAOB estimates were produced by Australian analysts for the Southern Ocean, and because of the geographical remoteness, are unlikely to interfere with this project. Finally, Kistler et al outlines a problem with the model's formulation of the horizontal moisture diffusion creating unreasonable snowfall over high-latitude valleys in the winter caused by moisture convergence. Due to the location, large scale nature of this study, and use of SLP only, it is unlikely this error will cause data problems for this study. Despite these limitations, the reanalysis is the most comprehensive database for use in studies such as this one.

Sea Level Pressure (SLP) is a class A output variable from the reanalysis and is used at both the monthly and daily temporal scales from 1948 to 2008 in this study.

The values taken from the reanalysis were run through a series of FORTRAN programs to create a vorticity value at each reanalysis grid point, leading to the results found in section 3. The monthly SLP values were also used to make composite difference figures for verification of the vorticity metric.

2.1.1 IABP Network

Figure 2.1 shows the number of observations for each reanalysis grid point from 1946 to 1998. There is a large increase in the number observations from 60°N to 90°N starting just before 1980. One reason for the increase is the dense buoy network, called the Arctic Buoy Ocean Network (later changed to International Arctic Buoy Programme), which began collecting synoptic scale pressure measurements over the Arctic Ocean in 1979. This buoy data produced never-before-available data on the Arctic, and has since been assimilated into the NCAR/NCEP Reanalysis (information taken from project website http://iabp.apl.washington.edu/).

The lack of observations prior to this network brings the quality of the 1948-1978 SLP data over the Arctic into question. Figure 2.2 compares the 1948-1978 and 1979-2008 time periods of seasonal climatological mean SLP. In examining each season, only differences of about 2hpa can be found in winter and summer, and these differences can be expected between 30-year periods due to natural variability. Thus the entire 61years is used in this study.

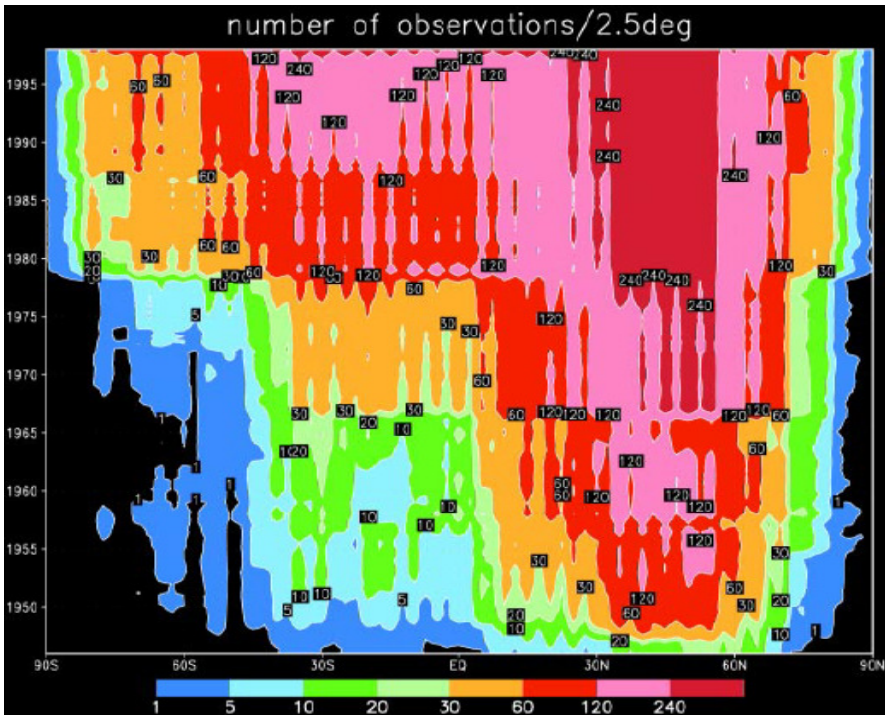

Figure 2.1: Zonal mean number of all types of observations per 2.5° lat–long box per month from 1946 to 1998 (taken from Kistler et al, 2001)

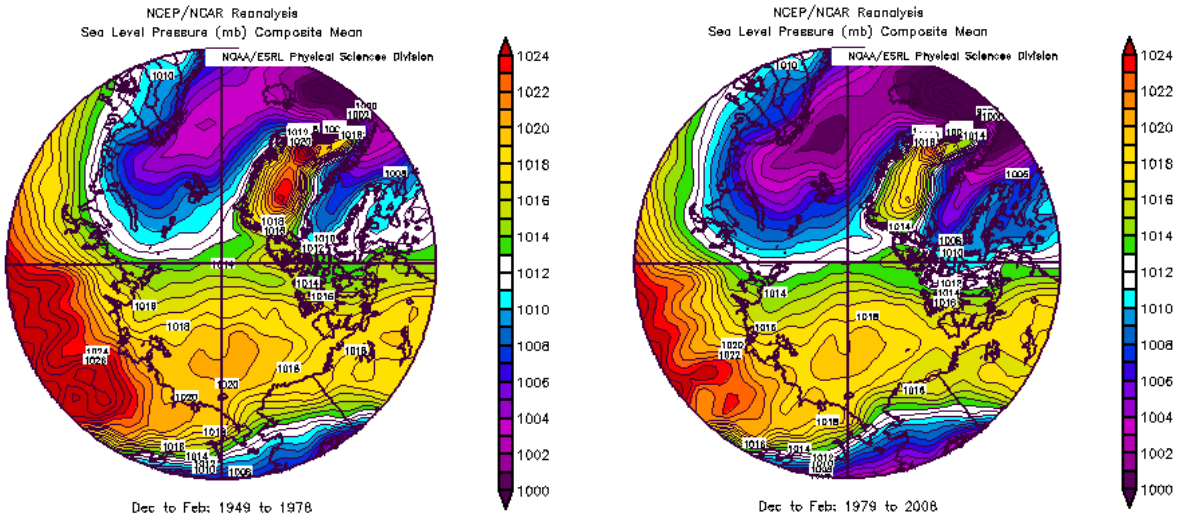

Figure 2.2(a): Winter NCAR/NCEP Reanalysis SLP from 60°N-90°N comparing the time periods 1948-1978 and 1979-2008.

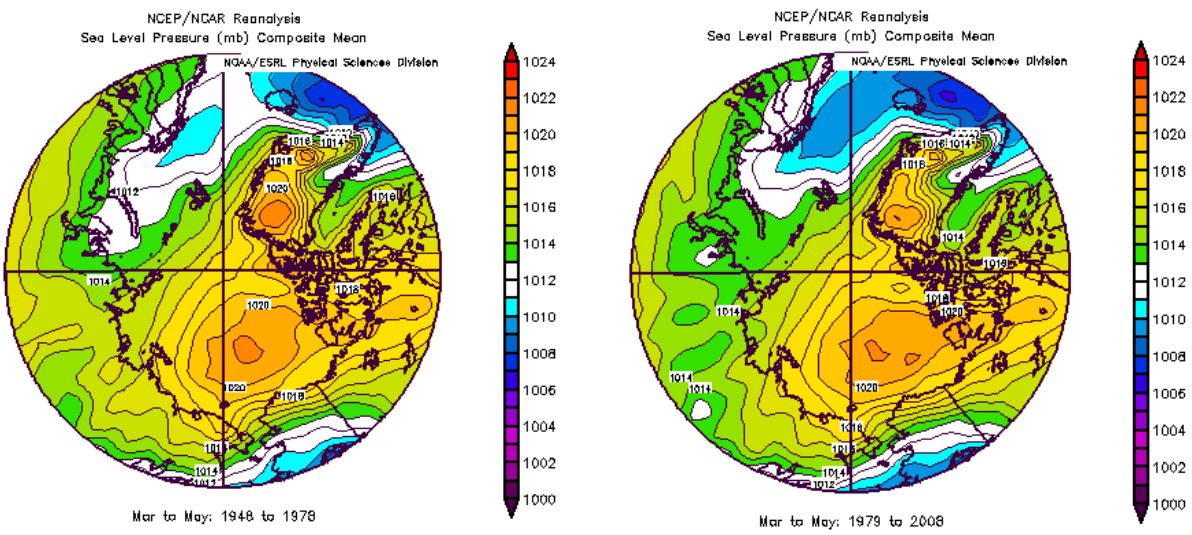

Figure 2.2(b): same as (a) except for spring

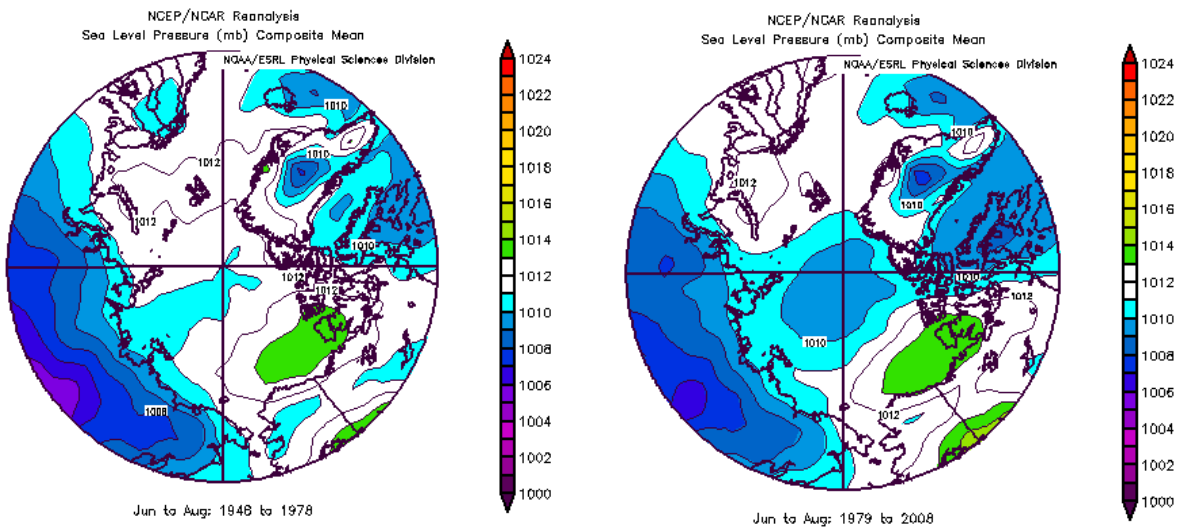

Figure 2.2(c): same as (a) except for summer

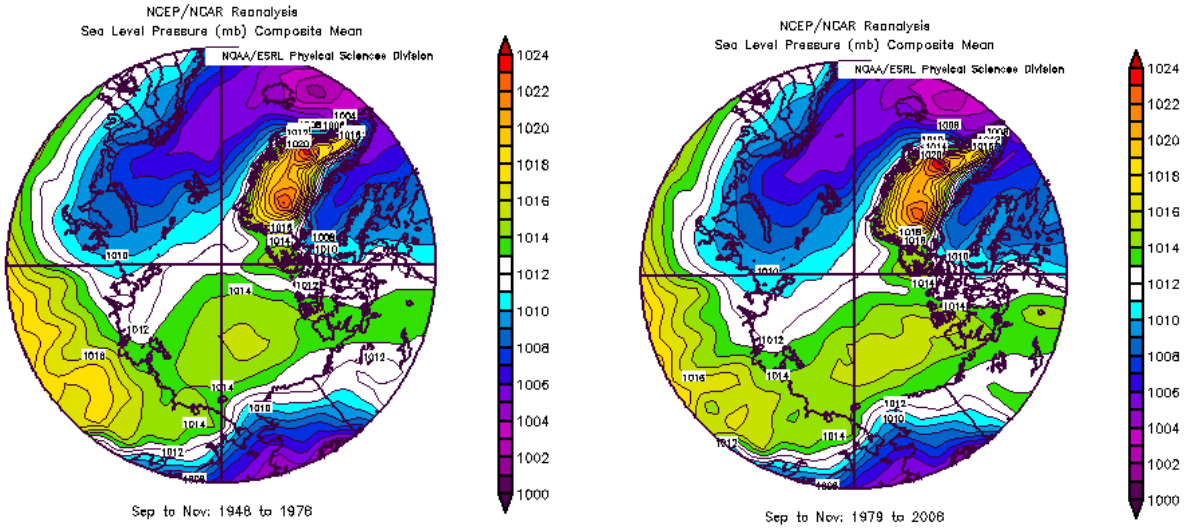

Figure 2.2(d): same as (a) except for autumn

2.2 Teleconnection Index Values

According to the Climate Prediction Center, a teleconnection is defined as a strong statistical relationship between weather in different parts of the globe, http://www.cpc.noaa.gov/products/outreach/glossary.shtml#T. For an understanding of the variability of the Beaufort Anticyclone, it is important to examine any possible relationships of known teleconnections on the Beaufort region.

Four teleconnections shown by previous studies to affect parts of the Arctic were included in this study: Arctic Oscillation (AO), Pacific North American (PNA), North Atlantic Oscillation (NAO), and Pacific Decadal Oscillation (PDO) (L'Heureux et al 2008, Wallace and Gutzler 1981, Rigor et al 2002, etc). The El Niño/Southern Oscillation (ENSO) is also included to examine any low latitude influences. Monthly values for the teleconnections were provided by the Climate Prediction Center (CPC) for the AO, PNA, NAO, and ENSO. The University of Washington's Joint Institute for the Study of the Ocean and Atmosphere, JISAO, (http://jisao.washington.edu/pdo/) provided the monthly values for the PDO.

The AO is defined as first Empirical Orthogonal Function (EOF) to the 1000hpa field poleward of 20°N. To create the index value the monthly mean 1000hPa height anomalies are projected onto the leading EOF mode. The index is normalized by the standard deviation of the monthly index from a base period (1979-2000) created from the NCAR/NCEP reanalysis. Figure 2.3 shows the positive phase of the AO having positive height anomalies over the northern Pacific and Atlantic with negative height anomalies over the Arctic Ocean. The negative phase would show the opposite signal.

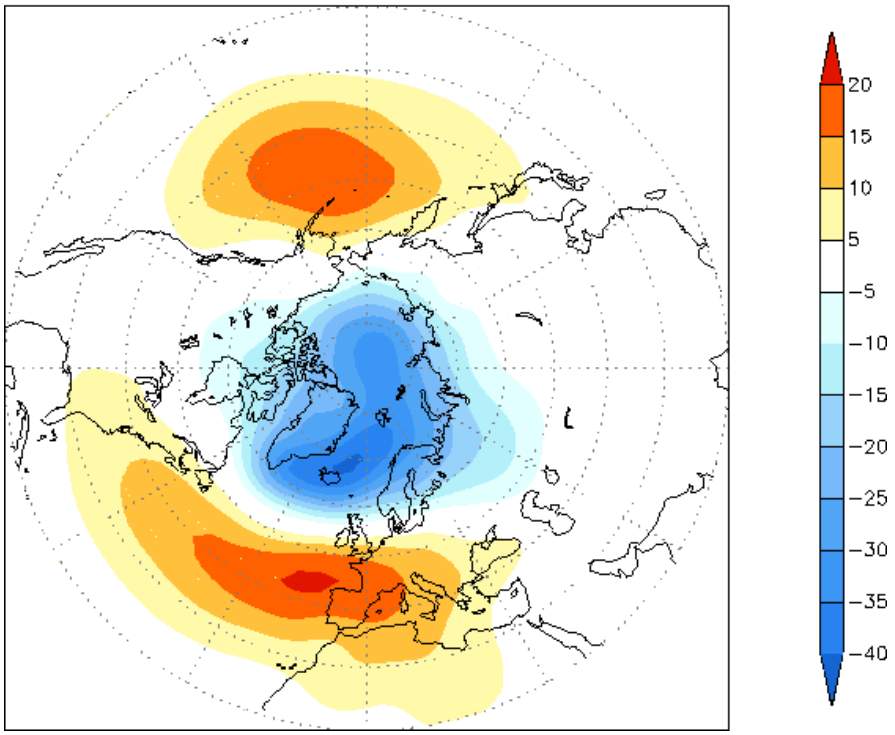

Figure 2.3: Leading EOF of 1000mb field shows positive phase of AO in terms of height anomalies in meters (Figure taken from CPC)

The PNA and NAO teleconnection index values are calculated similarly by the CPC using the Rotated Principal Component Analysis (RPCA) (Barnston and Livezey, 1987). This procedure isolates the primary teleconnection patterns for all months and allows time series of the patterns to be constructed. The RPCA technique is applied to the monthly mean standardized 500hpa height anomalies obtained from the NCAR/NCEP Reanalysis in the analysis region 20°N-90°N between January 1950 and December 2000. The anomalies are standardized by the 1950-2000 base period monthly means and standard deviations. Figure 2.4 shows the positive phase of the PNA (a) having negative height anomalies in the northern Pacific Ocean, with a weaker signal in July and the NAO (b) having negative height anomalies in the northern Atlantic Ocean and positive anomalies in the central Atlantic. The negative phases of these patterns would show the opposite signals.

The PDO is defined as the first EOF of the sea surface temperature anomalies (SSTAs) poleward of 20 °N latitude. The PDO index is created using the SSTAs in the Pacific Ocean. Figure 2.5 shows the positive phase of the PDO with negative SSTAs over the northern Pacific Ocean. The negative phase would show the opposite signal.

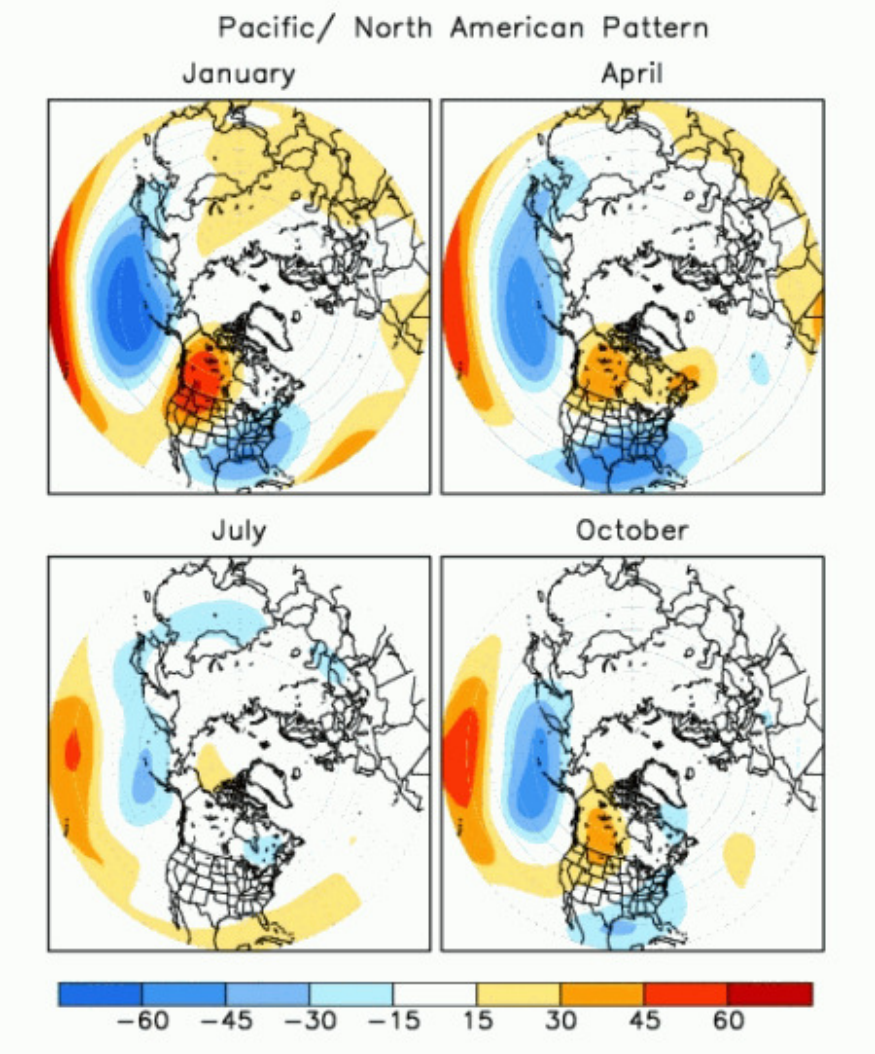

Figure 2.4(a): PNA teleconnection pattern showing height anomalies in meters associated with the positive phase for each season (Figure taken from CPC)

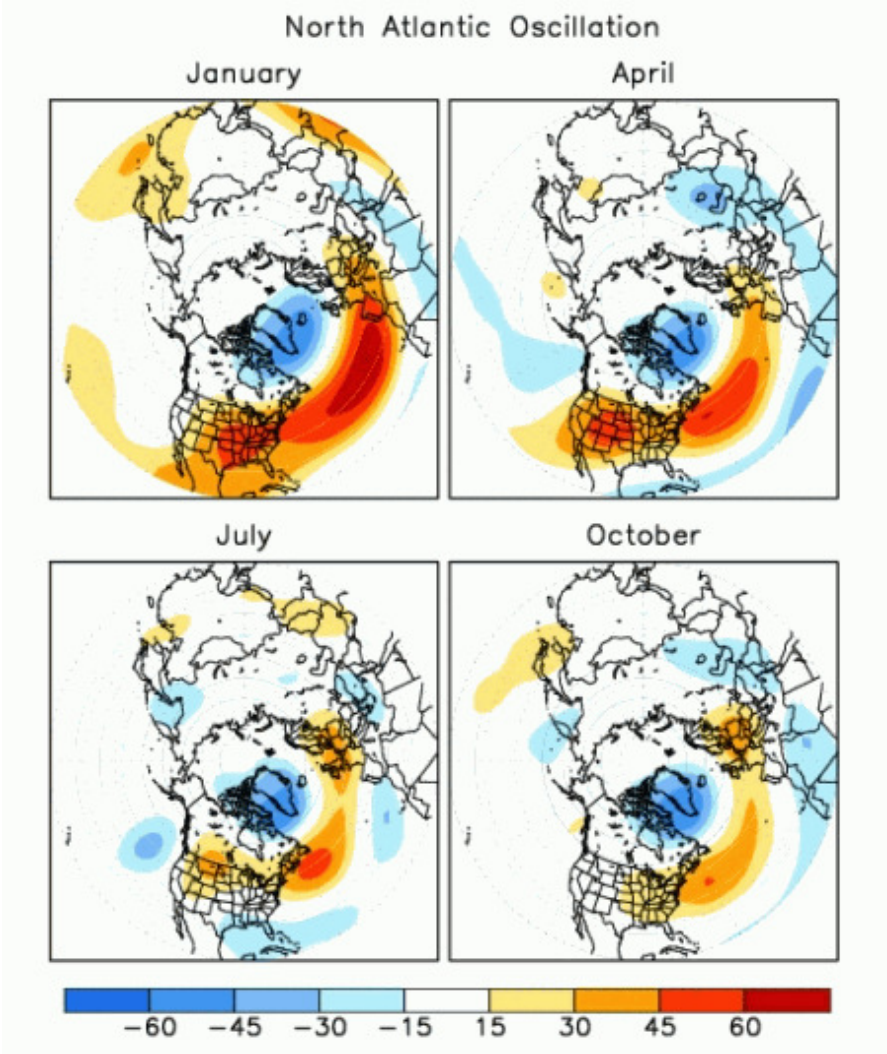

Figure 2.4(b): NAO teleconnection pattern showing height anomalies in meters associated with the positive phase for each season (Figure taken from CPC)

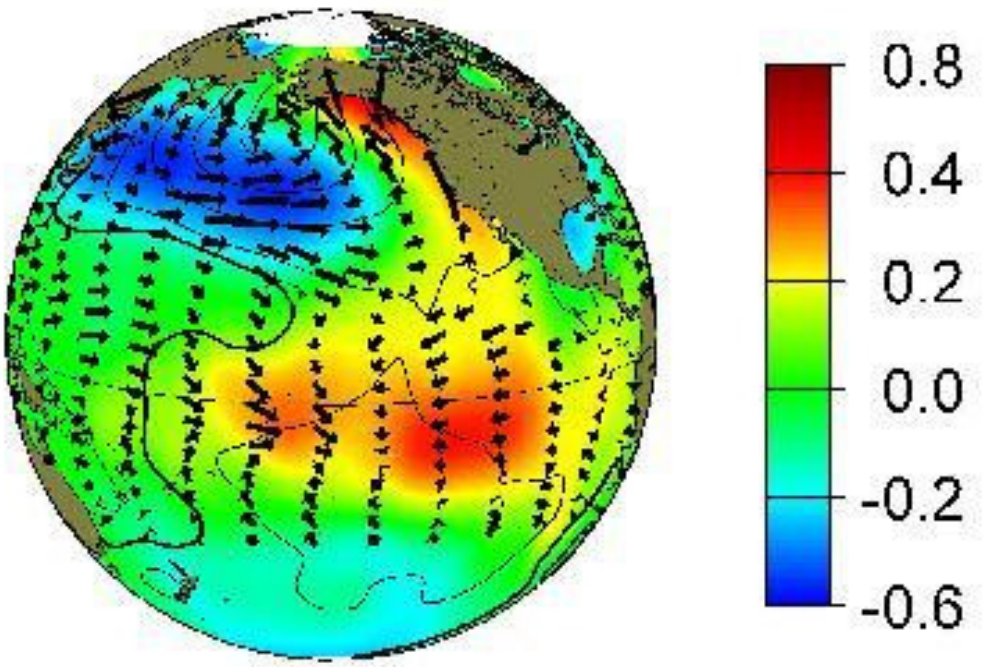

Figure 2.5: PDO in positive phase showing SSTAs (color), SLP (contours), and surface wind stress (arrows) (Figure taken from http://jisao.washington.edu/pdo/)

The Bivariate ENSO Timeseries index (Smith and Sardeshmukh, 2000) was chosen for tracking the ENSO pattern. It considers both the atmospheric and oceanic components of ENSO by using Southern Oscillation Index (SOI) and Nino 3.4 SST (SST of region from 5˚ N to 5˚ S and 170˚ W to 120˚ W). The SOI from 1855 - 1997 is from Climate Research Unit, and later indices are taken from the Climate Prediction Center. The SST data is from Global Ice and Sea Surface Temperature dataset (Rayner et al, 2006) up to April 1998, and later data is from the Reynolds SST dataset (Reynolds, 1988). The data is extracted from the 1898 – 2000 monthly average climatology and are standardized by month, after which a monthly index value is calculated from the combination of the SOI and SST for a given month. Figure 2.6 shows ENSO correlations in its positive phase to (a) SST, showing that when ENSO is positive, there are positive SST anomalies in the tropical Pacific, and (b) SLP, showing that when ENSO is positive, SLP is lower over the eastern Pacific and higher over the western Pacific. The opposite pattern would be valid for the negative phase of ENSO.

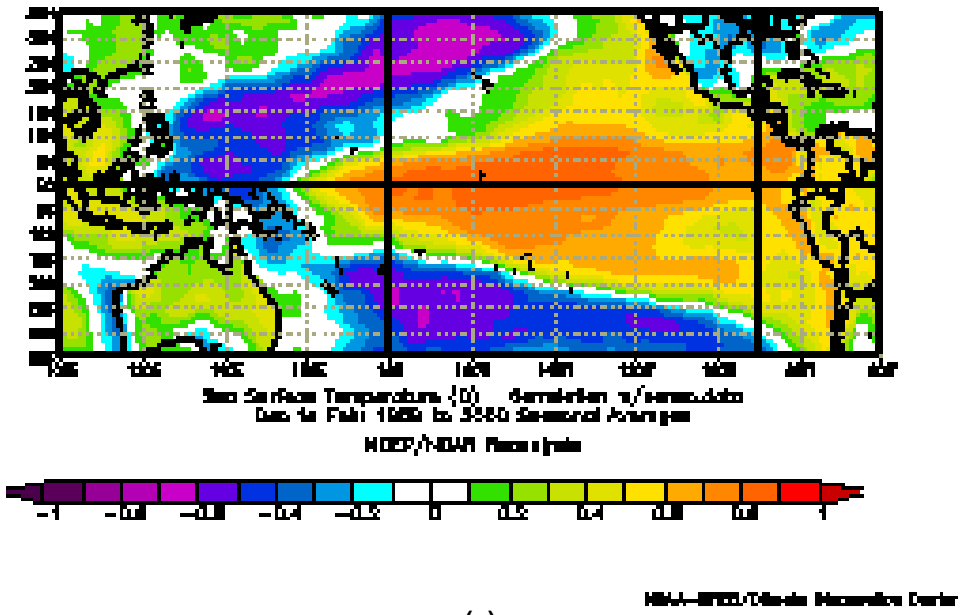

(a)

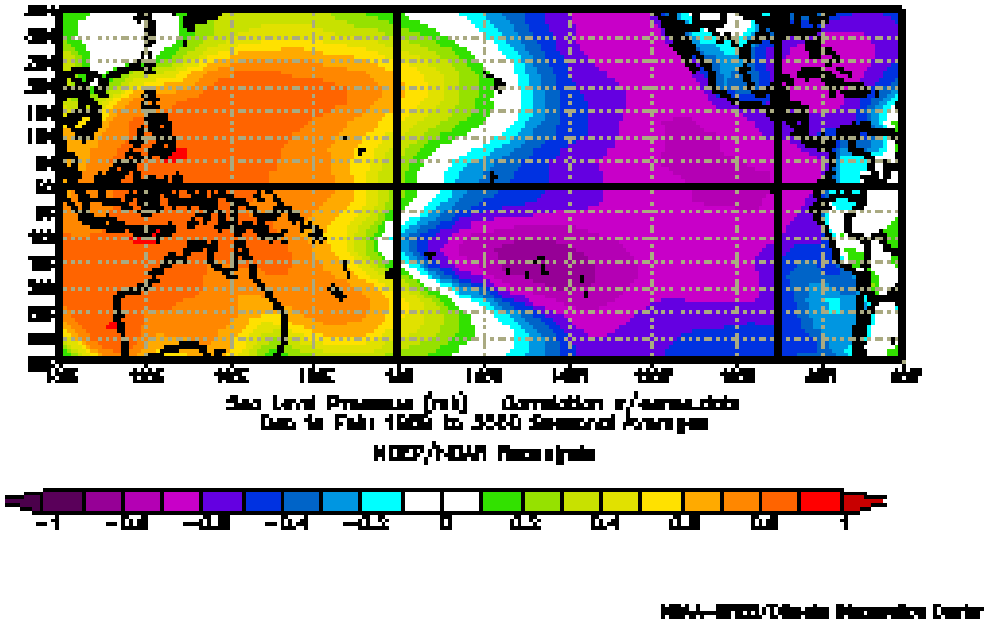

(b)

Figure 2.6: Correlations between the positive ENSO phase and (a) SST and (b) SLP (Figure taken from http://www.esrl.noaa.gov/psd/people/cathy.smith/best/)

Along with the large spatial patterns of the teleconnections, there is also a highly variable temporal signal. As shown in figure 2.7, the PDO (a) and AO (b) are shown to display how different teleconnection patterns can have drastically different temporal signals. The smoothed PDO timeseries shows shifts between the positive and negative phases on the timescale of years. The 3 month running mean signal of the AO signal appears to shift phases throughout the annual time frame.

2.3 NCAR Graphics

The NCAR Graphics library, http://ngwww.ucar.edu/, was the main source to create figures for this project. It was selected for its ability to draw contours and maps using FORTRAN, the main method of data manipulation.

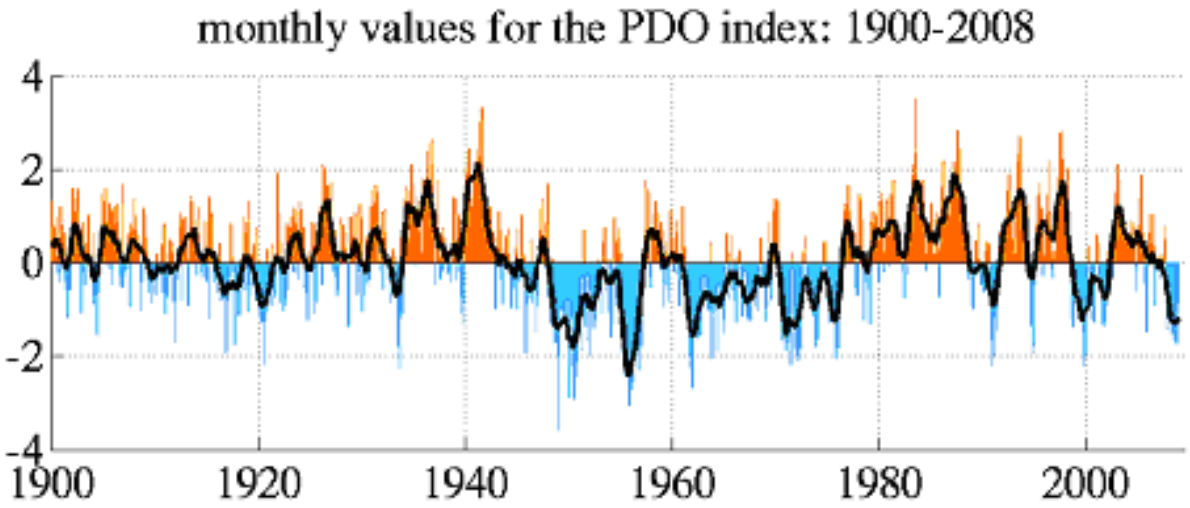

Figure 2.7(a): Timeseries of PDO teleconnection values taken from http://jisao.washington.edu/pdo/

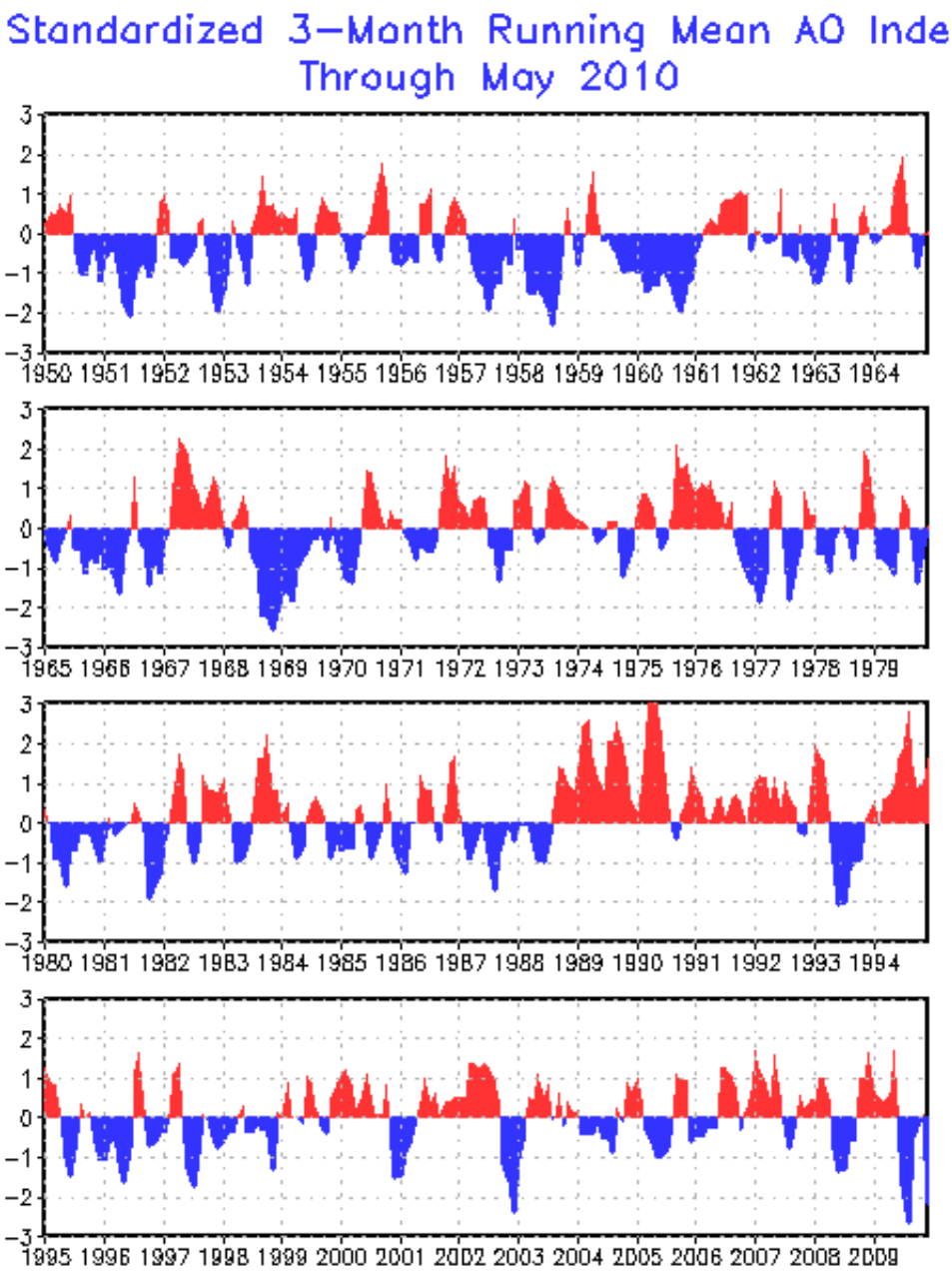

Figure 2.7(b): Timeseries of AO teleconnection values taken from CPC

3. Methods and Results

3.1 Metric of the Beaufort Anticyclone

In order to characterize the magnitude of the Beaufort Anticyclone, a vorticity metric was calculated using SLP from the NCAR/NCEP reanalysis. Vorticity provides an advantage over SLP due to vorticity's sensitivity to small pressure gradients, ease of determining features from background noise, and direct relation to the wind speed (Mesquita et. al, 2010).

Given geostrophic vorticity:

$$\xi = (\frac{\partial v}{\partial x} - \frac{\partial u}{\partial y}) \tag{1}$$

where v and u are the geostrophic winds:

$$v = \frac{1}{\rho f}(\frac{\partial p}{\partial x}) \qquad \text{and} \qquad u = \frac{-1}{\rho f}(\frac{\partial p}{\partial y}) \tag{2}$$

Where p is SLP, ρ is density, f is the Coriolis parameter, and neglecting the $(\frac{\partial f}{\partial y})$ term, vorticity can then be related to SLP by combining (1) and (2):

$$\xi = \frac{1}{\rho f}(\frac{\partial^2 p}{\partial x^2} + \frac{\partial^2 p}{\partial y^2}) \tag{3}$$

Using equation (3), vorticity was calculated for each reanalysis grid point for each month directly from the SLP values. Grid point vorticities were then averaged over the Beaufort Sea region in two ways. The first method was an areal average over 70°-90°N, 90°-270°W. This area was chosen as it encompasses the Beaufort Anticyclone's climatological location. The second method was a refinement of the first

method averaging the area centered on 75°N, 210°W, the climatological center, with a radius of 555 km or 5° latitude.

In order to illustrate the relationship between the vorticity metric and SLP, the averaged vorticity is correlated to the SLP at each reanalysis grid point using equation (4) for the correlation coefficient:

$$r = \frac{\sum_{i=1}^{n}((x_i - \bar{x})(y_i - \bar{y}))}{\sqrt{\sum_{i=1}^{n}(x_i - \bar{x})^2 \sum_{i=1}^{n}(y_i - \bar{y})^2}} \qquad (4)$$

Where x is vorticity, y is SLP and $\bar{x}$ and $\bar{y}$ are the corresponding monthly mean values.

Figure 3.1 compares the two method's area used to average the vorticity metric. In comparing figure 3.1(a) to 3.1(b) only small differences are found in the correlation signal. However, the second method refined the averaged area to the climatological mean location of the Beaufort Anticyclone, making it the preferred method for this study.

A closer inspection of figure 3.1 shows the vorticity and SLP correlations averaged at the annual timescale producing areas of higher correlations south of Alaska and north of Siberia opposite to the signal produced by the Beaufort Anticyclone. In order to further investigate the findings in figure 3.1, the annual cycle was removed by subtracting the climatological values for each month; the climatology is discussed in detail later in this section. Figure 3.2(a) shows the annual correlation with the annual cycle removed. Even with the annual cycle removed, the higher correlation areas south of Alaska and north of Siberia remain as the dominate

correlation features. A breakdown of figure 3.2(a) into seasonal correlations is shown in figure 3.2(b)-(e), the dominant correlation features as seen in figure 3.2(a) are present in all seasons. This pattern is consistent with conclusions of Serreze et. al 1993. They found a decrease in anticyclone activity over Siberia and Alaska occurs with an increase of pressure over the Beaufort region.

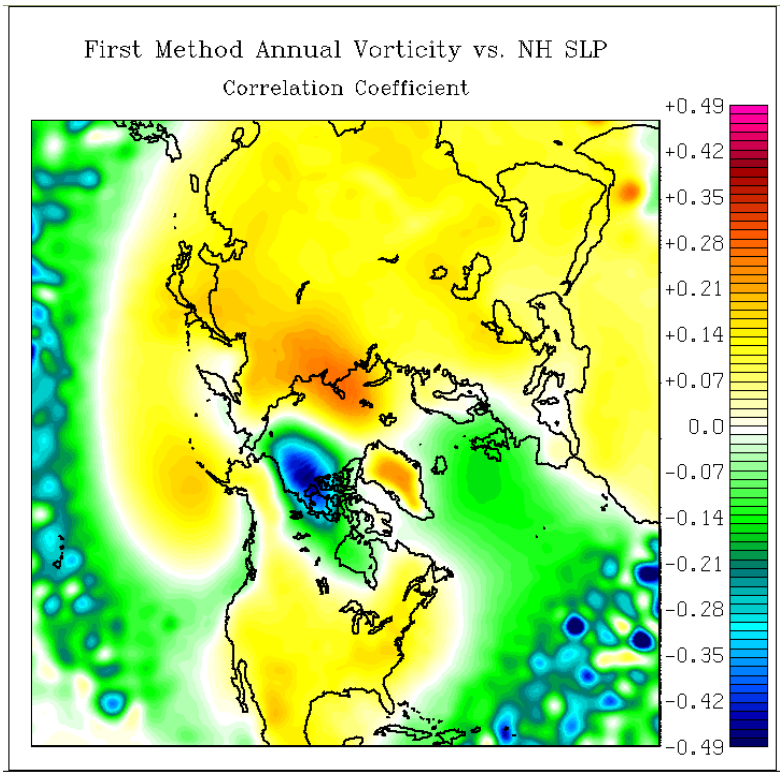

Figure 3.1(a): Annual correlation map of vorticity averaged over the Beaufort Sea and NH SLP using the first method

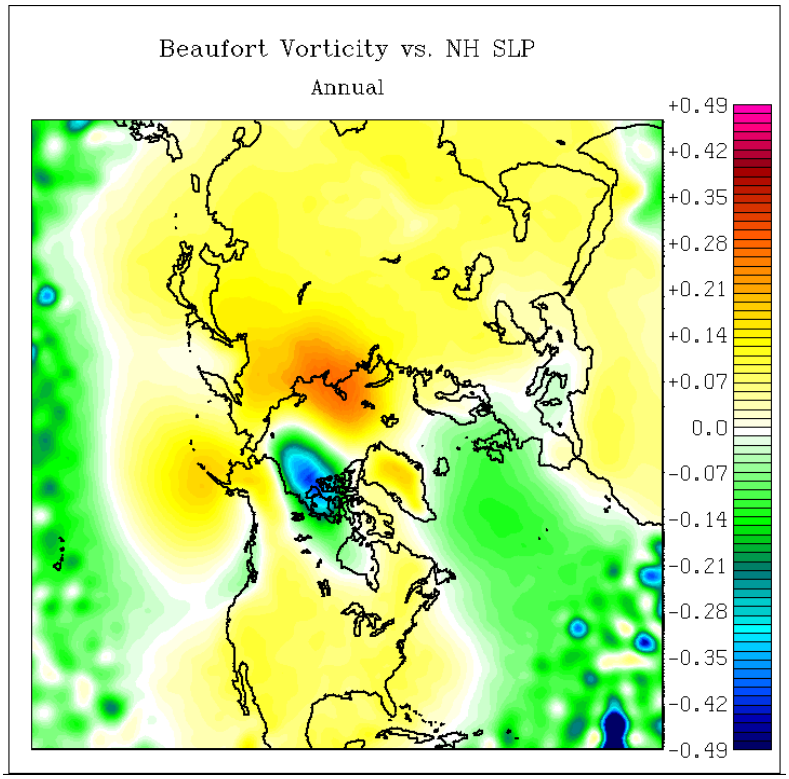

Figure 3.1(b): same as (a) but using the second method

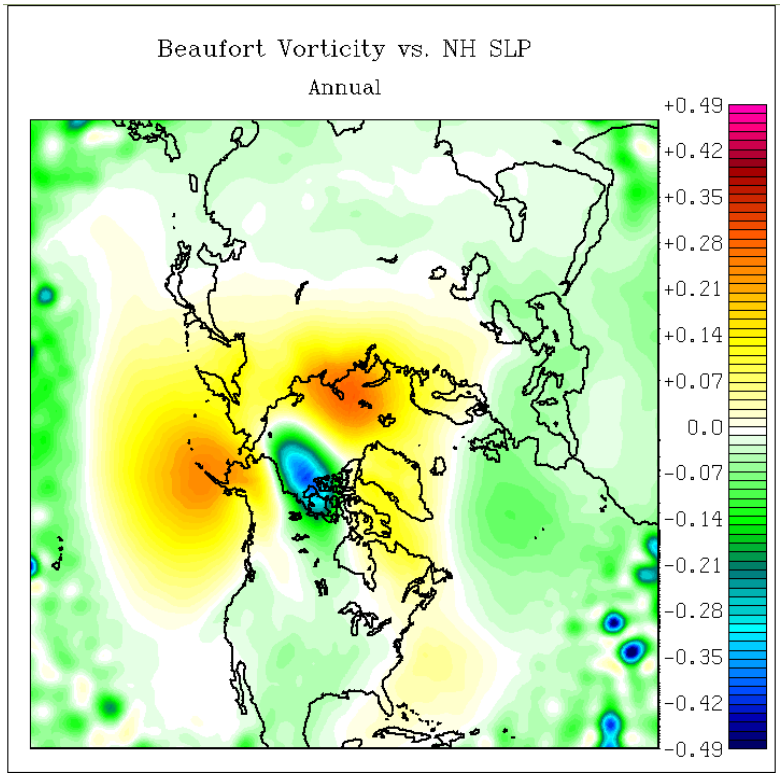

Figure 3.2(a): Annual Beaufort vorticity correlation with NH SLP with annual cycle removed. Based on vorticity averaged using second averaging method

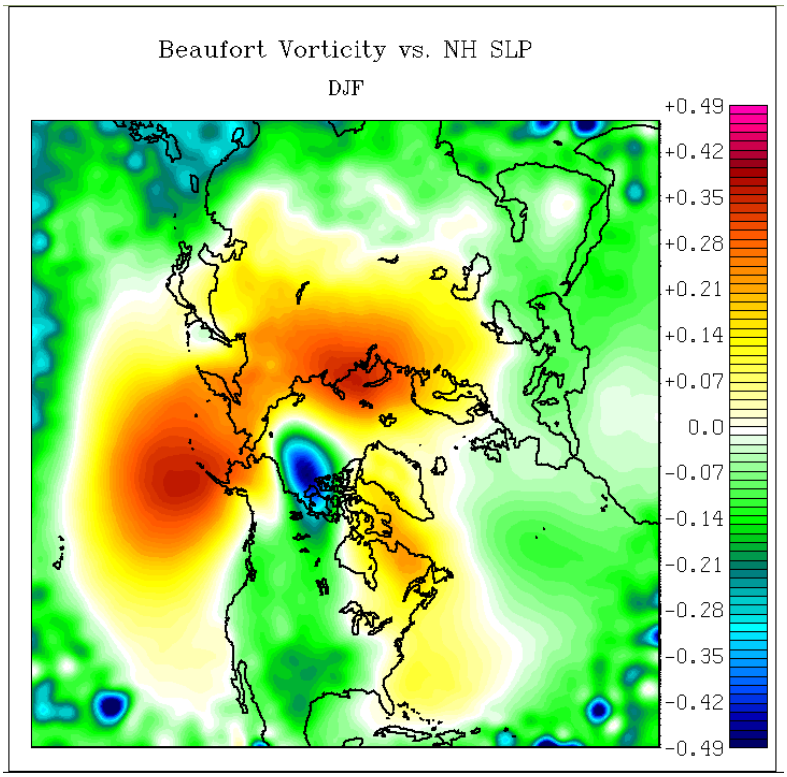

Figure 3.2(b): Seasonal Beaufort vorticity correlation with NH SLP with annual cycle removed for winter

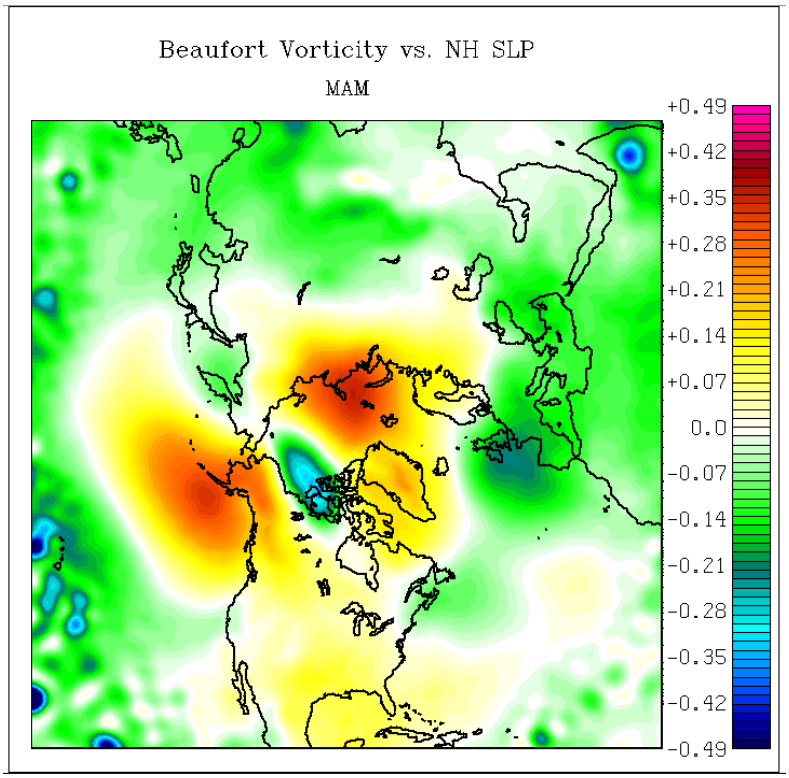

Figure 3.2(c): same as (b) but for spring

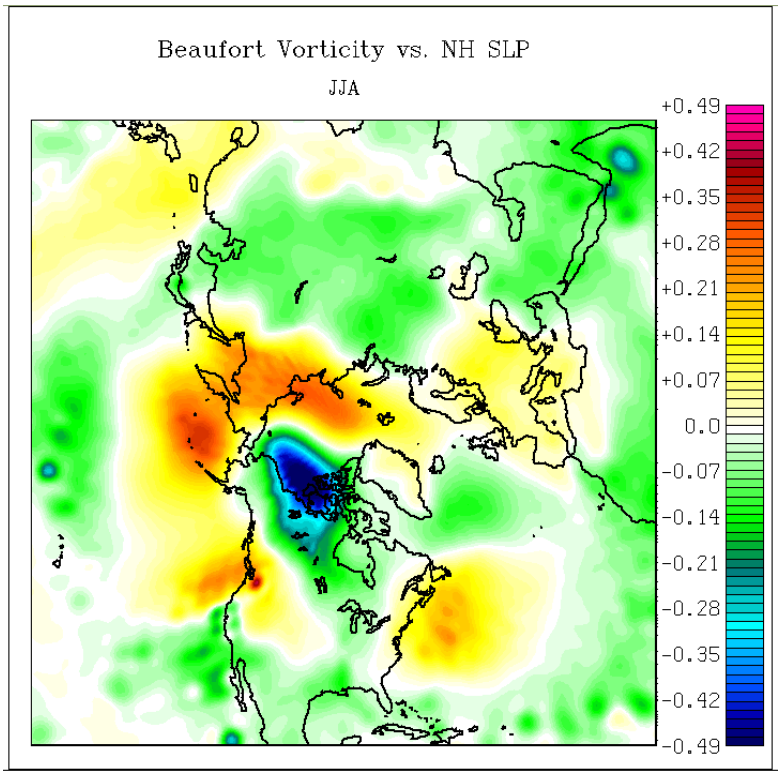

Figure 3.2(d): same as (b) but for summer

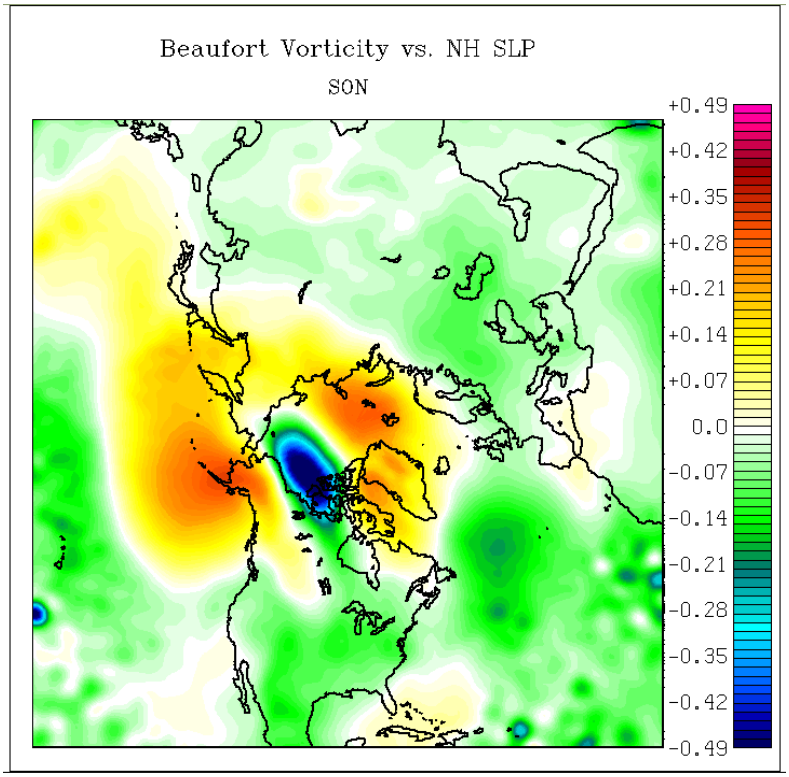

Figure 3.2(e): same as (b) but for summer

3.1.1 Significance Testing

Significance of the correlation signal was tested using a Monte Carlo significance technique. SLP values were temporally randomized 1000 times and correlated with the averaged vorticity. The randomized values were sorted from smallest correlation to largest correlation. The original correlations are considered significant at the 90% level if the original values are greater than the 950 randomized value or less than the 50 randomized value. Figure 3.3 shows the vorticity correlations with regions of 90% significance areas shaded. The annual figure shows a large area of significance that mixes the seasonal patterns, which show a more interesting signal. In general, the seasonal breakdown shows more significance in the Pacific Ocean than the Atlantic, which has implications for teleconnection influences that will be described later in this section. Also, the annual and all seasons show significance in the correlation signal over Northern Siberia and Southern Alaska.

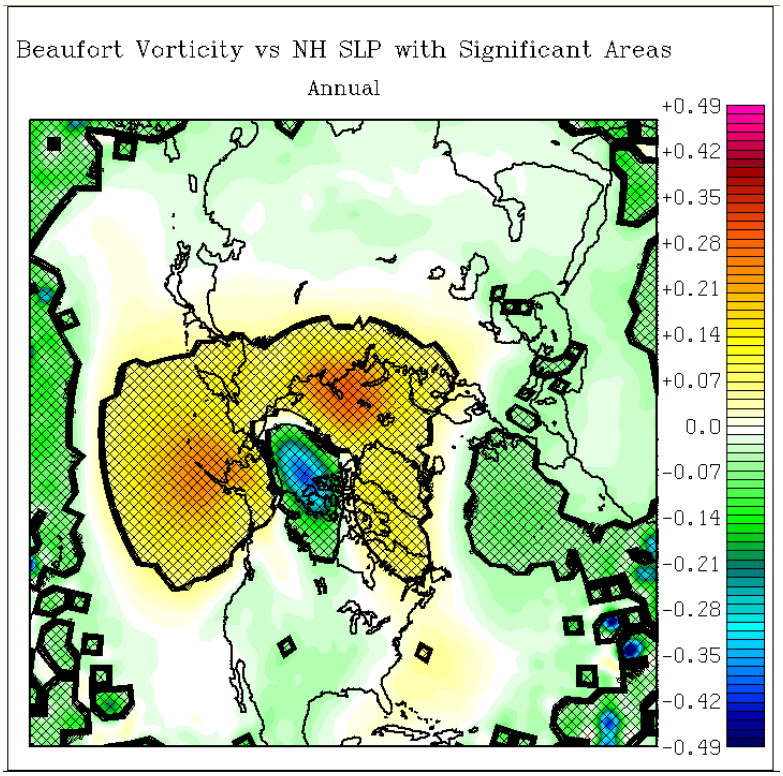

Figure 3.3(a): Same annual correlation shown in figure 3.2(a) with areas of 90% significance shaded in black

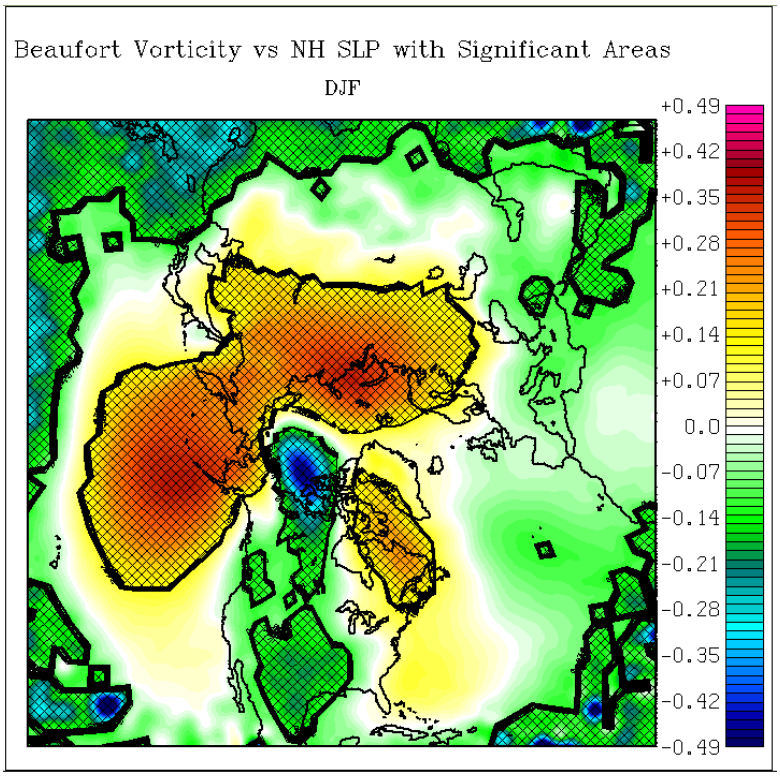

Figure 3.3(b): Same seasonal correlations shown in figure 3.2(b) with areas of 90% significance shaded in black for winter

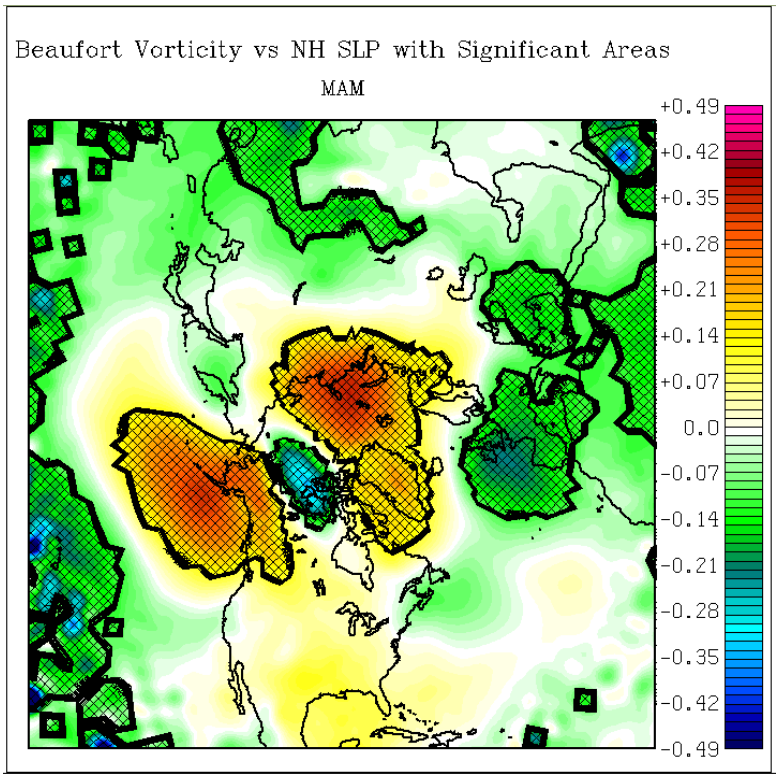

Figure 3.3(c): Same seasonal correlations shown in figure 3.2(c) with areas of 90% significance shaded in black for spring

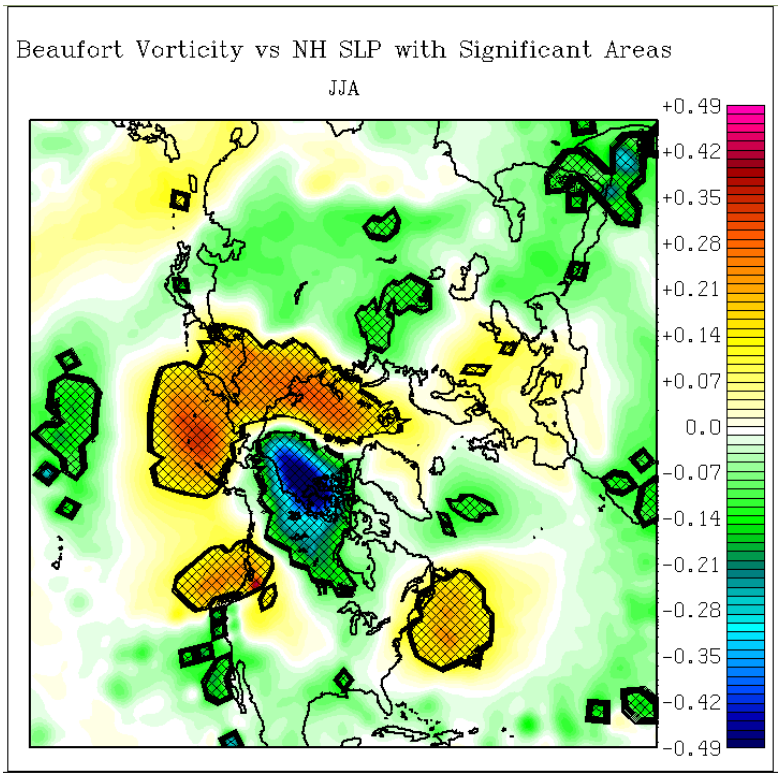

Figure 3.3(d): Same seasonal correlations shown in figure 3.2(d) with areas of 90% significance shaded in black for summer

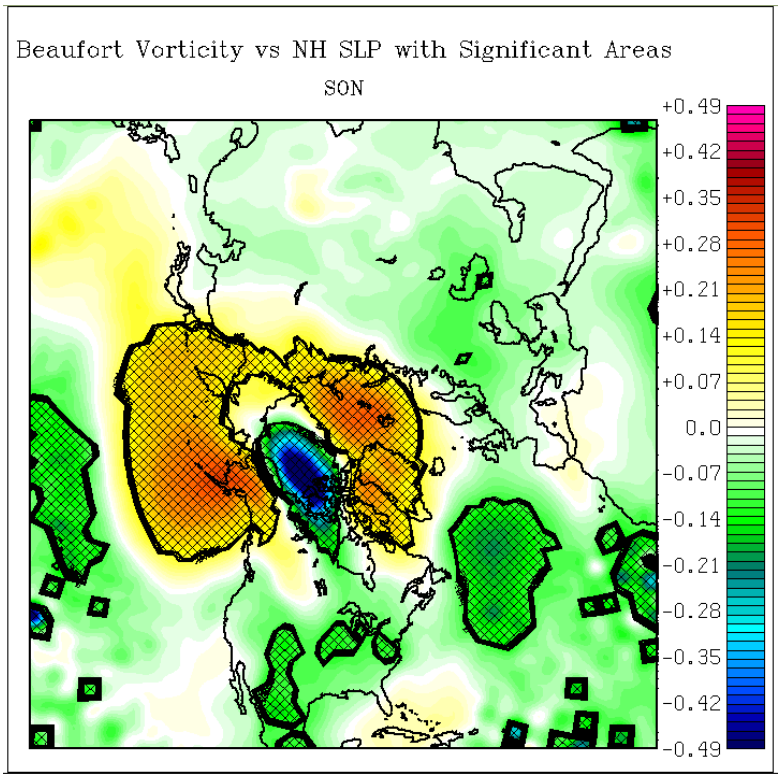

Figure 3.3(e): Same seasonal correlations shown in figure 3.2(e) with areas of 90% significance shaded in black for autumn

3.1.2 Justification for Vorticity Metric

In order to justify the use of vorticity in this study, the same averaging and correlation method was followed using SLP. The results of the SLP correlations are shown in figure 3.4. In the annual and seasonal breakdown, a large area of positive correlation exists over a large area of the Arctic Ocean, with the maxima occurring over the Beaufort region. The annual correlation shows areas of negative correlation in both the Pacific and Atlantic Oceans. This signal is most likely an average of the seasonal signals because there is an area of higher negative correlations over the Atlantic Ocean in spring and Pacific Ocean in autumn. This provides an interesting result as it supports the 'see-saw' theory of Cullather and Lynch 2003 who showed a transfer of mass from the Atlantic Ocean to the Pacific Ocean via the Arctic Ocean during spring and from the Pacific Ocean to Atlantic Ocean during autumn. Atlantic Ocean and Pacific Ocean connection is also relevant in the AO teleconnection pattern, supporting previous studies (Rigor et al, 2002) of interactions between the Beaufort Anticyclone and the AO. It is also interesting to note that the features south of Alaska and north of Siberia are not found in any of the correlations, even though these were prominent in the vorticity-based correlations. Therefore, by using vorticity to track the Beaufort Anticyclone; smaller scale features are being found. The features may be attributed to vorticity's sensitivity to changes in the pressure gradient, either by increasing/decreasing the Beaufort Anticyclone magnitude or a change in the anticyclone's position.

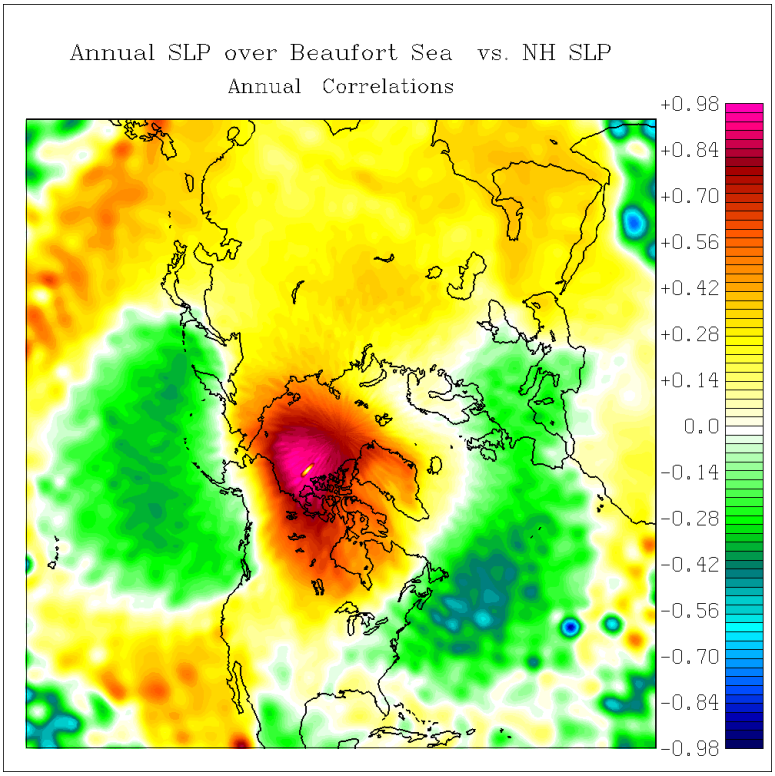

Figure 3.4(a): Annual SLP averaged over Beaufort Sea correlated with NH SLP

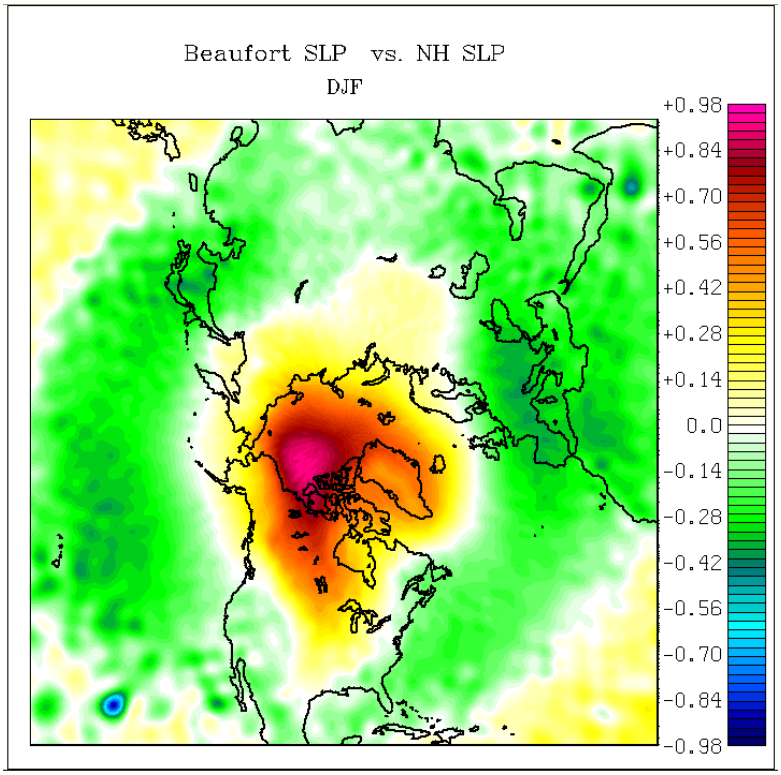

Figure 3.4(b): Same as 3.4(a) but for winter

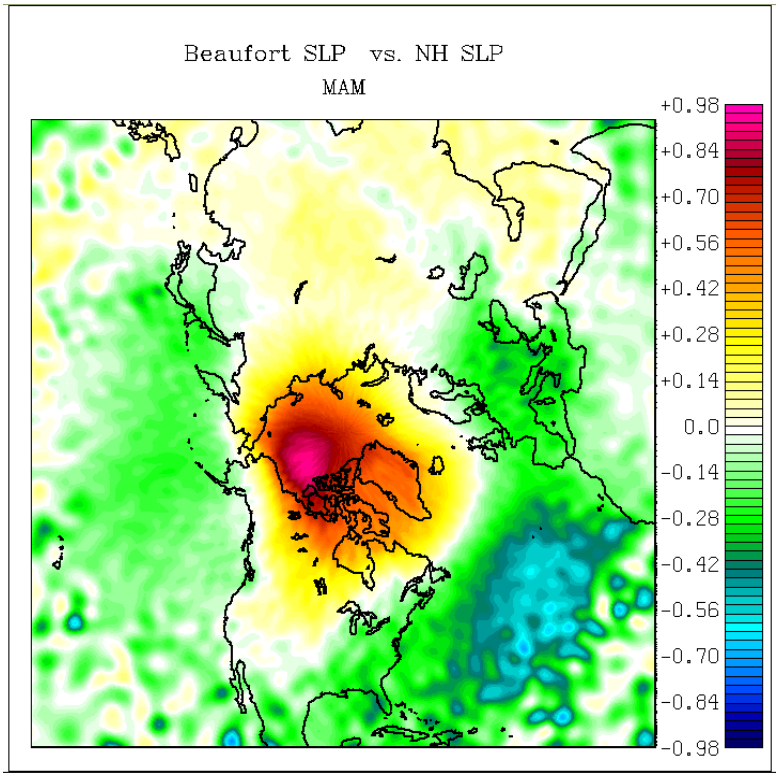

Figure 3.4(c): Same as 3.4(a) but for spring

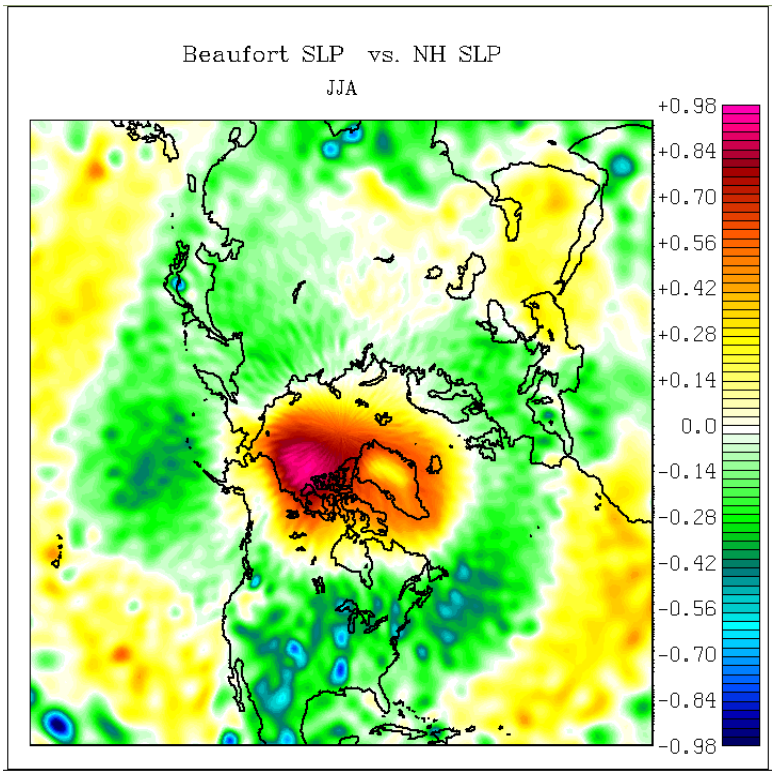

Figure 3.4(d): Same as 3.4(a) but for summer

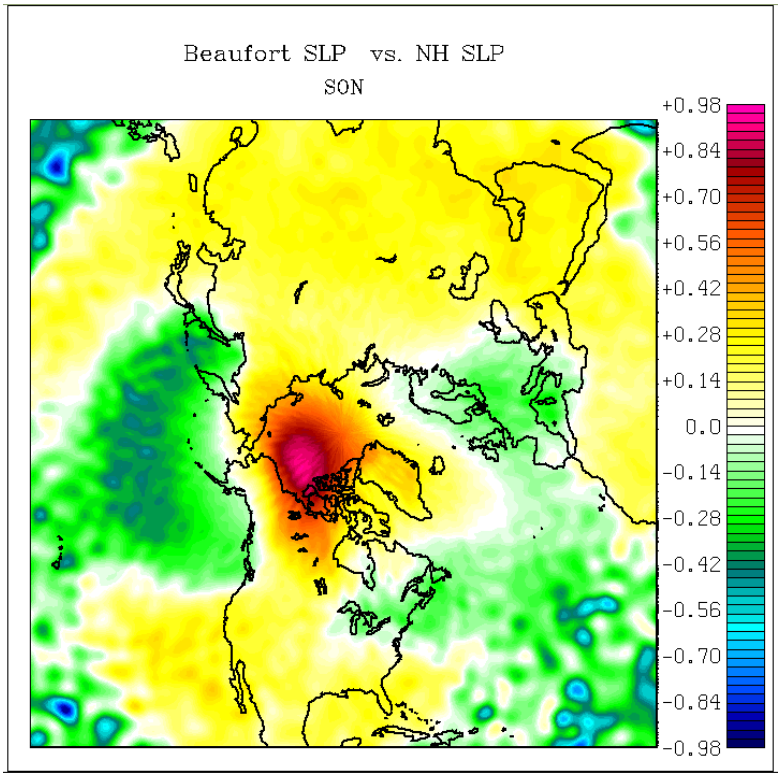

Figure 3.4(e): Same as 3.4(a) but for autumn

3.1.3 Signature of Vorticity Metric

In order to verify whether the vorticity metric is capturing an accurate signature of SLP variations, composite difference figures of SLP were created. Figure 3.5 shows a seasonal timeseries breakdown of the vorticity metric. Composite differences of SLP were created using the timeseries shown in figure 3.5. The 4 most extreme positive and negative years were selected from these timeseries and using the NCEP reanalysis Earth System Research Laboratory (ESRL) website (www.esrl.noaa.gov*)* the fields were plotted as the mean SLP fields for the mean SLP fields for the most extreme negative years minus the most extreme positive years. The results are shown in figure 3.6.

A comparison of figures 3.2 and 3.6 show a strong similarity in each season's signal. There is strong positive correlation in the vorticity in the same location as a decrease in pressure in the composite SLP difference. The opposite is true as well; there is strong negative correlation in the vorticity where there is an increase in the pressure in the composite SLP difference. Due to the similarity in the vorticity correlation and SLP composites, it is safe to assume the vorticity metric is capturing an accurate signal within the SLP. What the signal means is an area that will need further investigation.

Given the results from figures 3.2 and 3.6, the question of why the SLP correlations shown in figure 3.4 missed the features south of Alaska and north of Siberia arises again. As stated in the previous section, the vorticity metric is sensitive to changes in the pressure gradient and may be capturing changes in the anticyclone's position and intensity causing the smaller scale features to show.

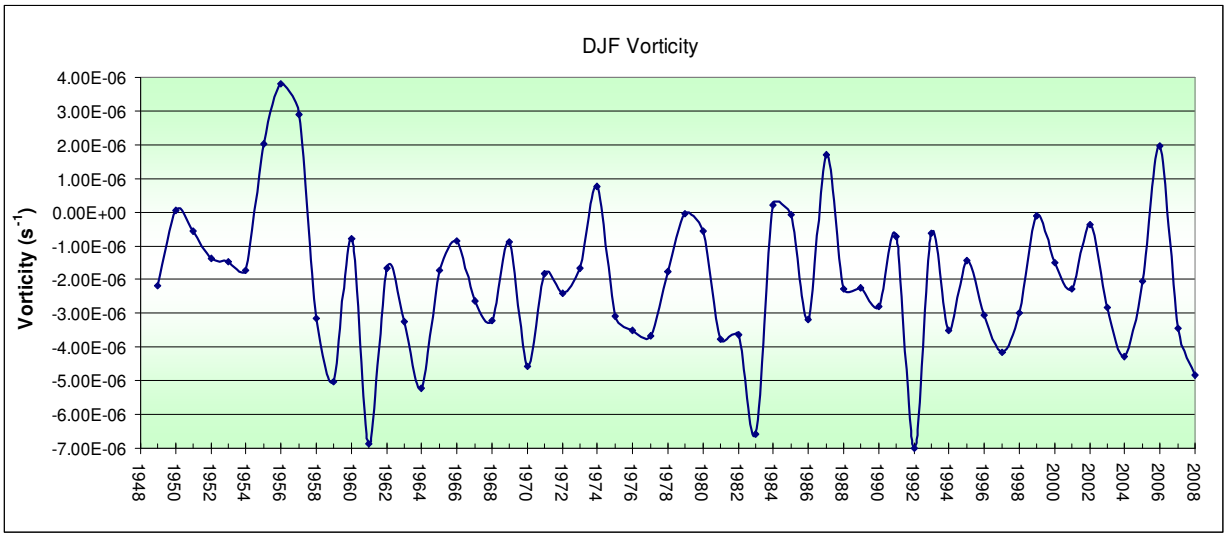

Figure 3.5(a): Winter timeseries of vorticity metric

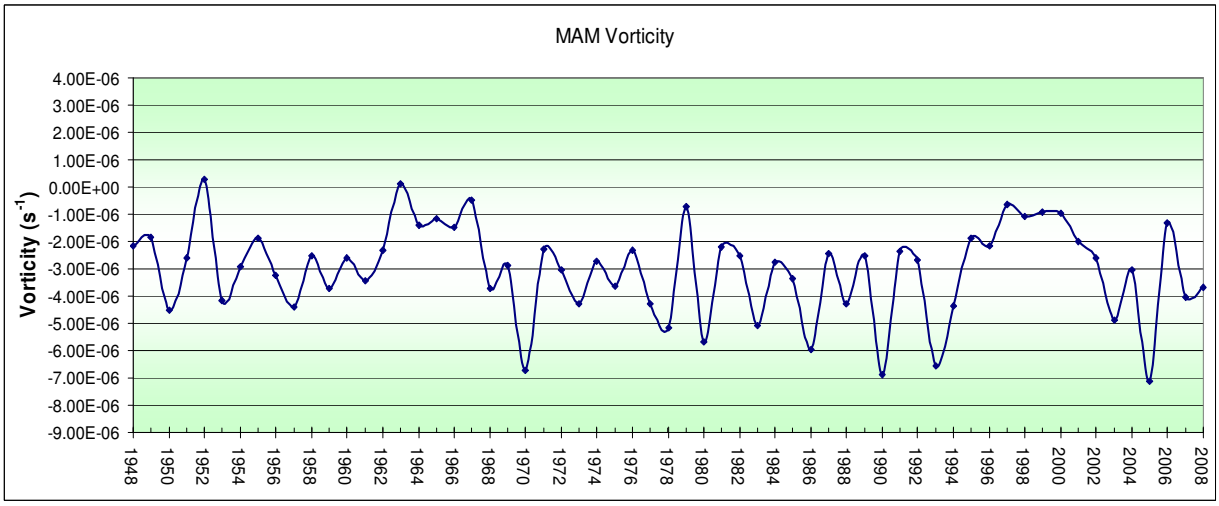

Figure 3.5(b): Spring timeseries of vorticity metric

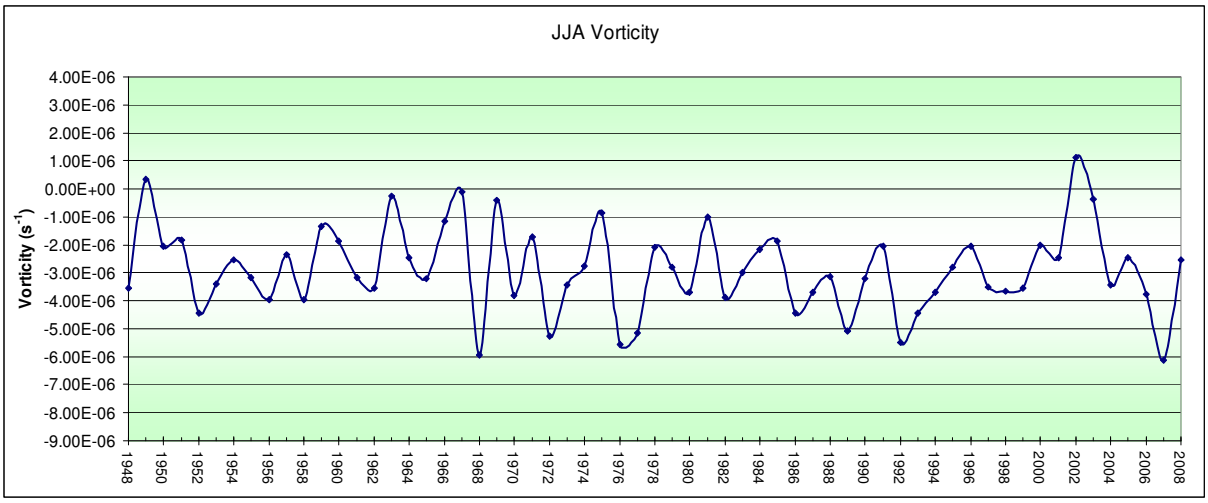

Figure 3.5(c): Summer timeseries of vorticity metric

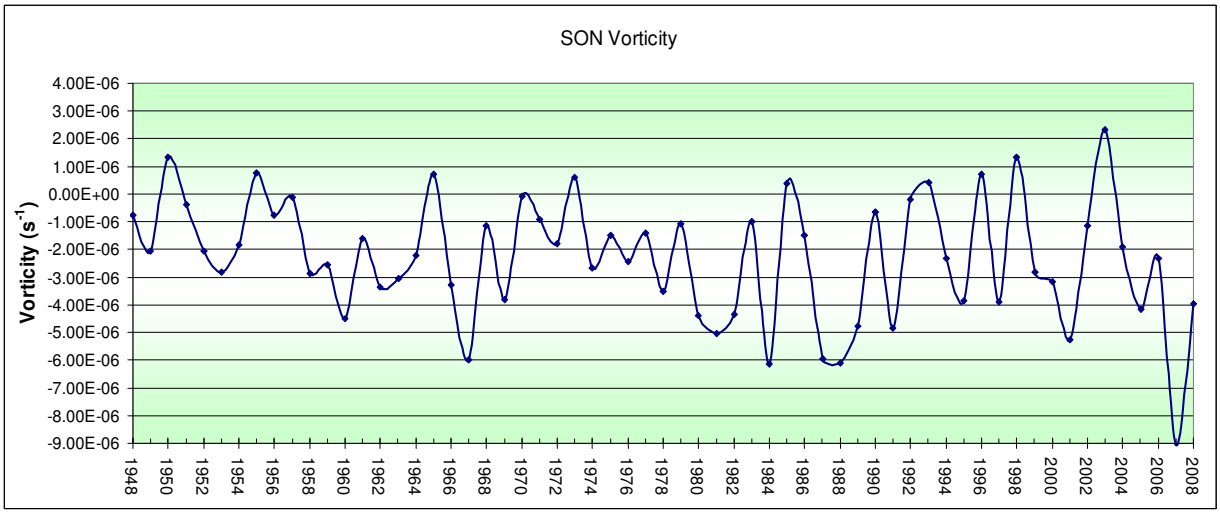

Figure 3.5(d): Autumn timeseries of vorticity metric

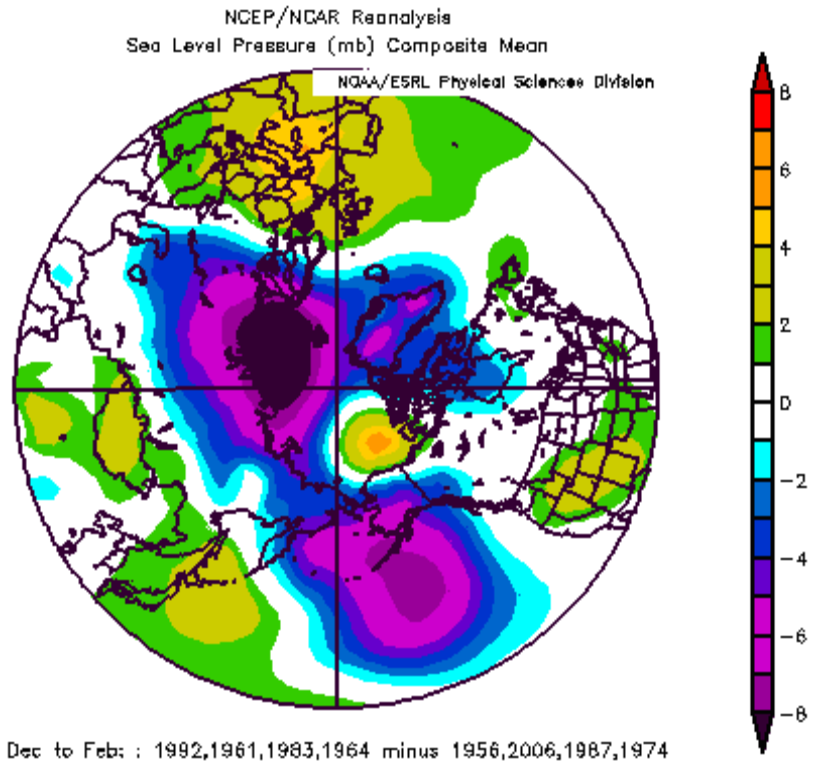

Figure 3.6(a): SLP composite differences of 4 most extreme negative years minus 4 most extreme positive years for winter from ESRL website, www.esrl.noaa.gov

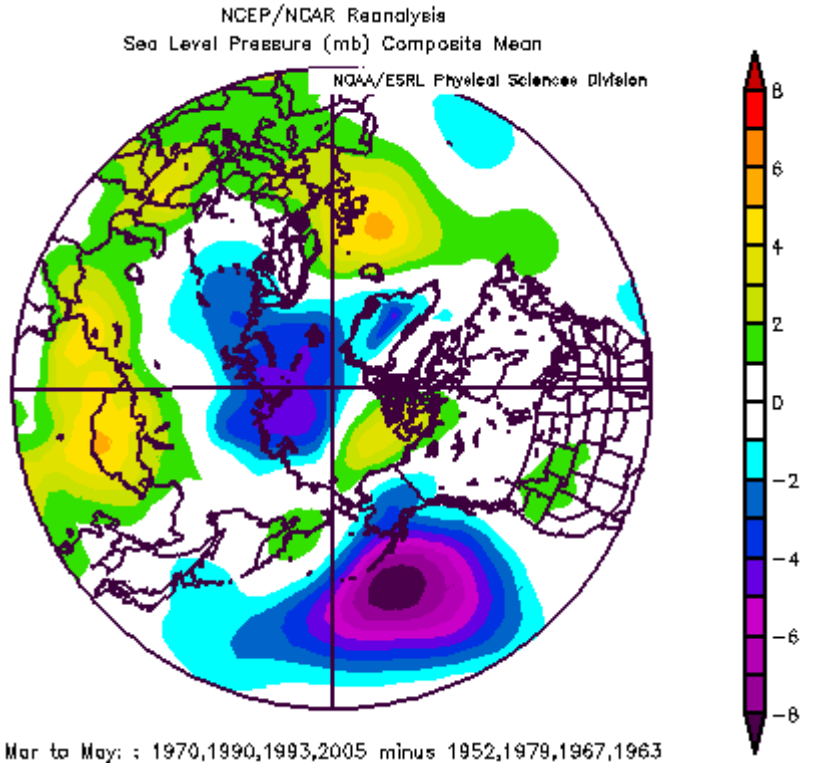

Figure 3.6(b): same as (a) but for spring

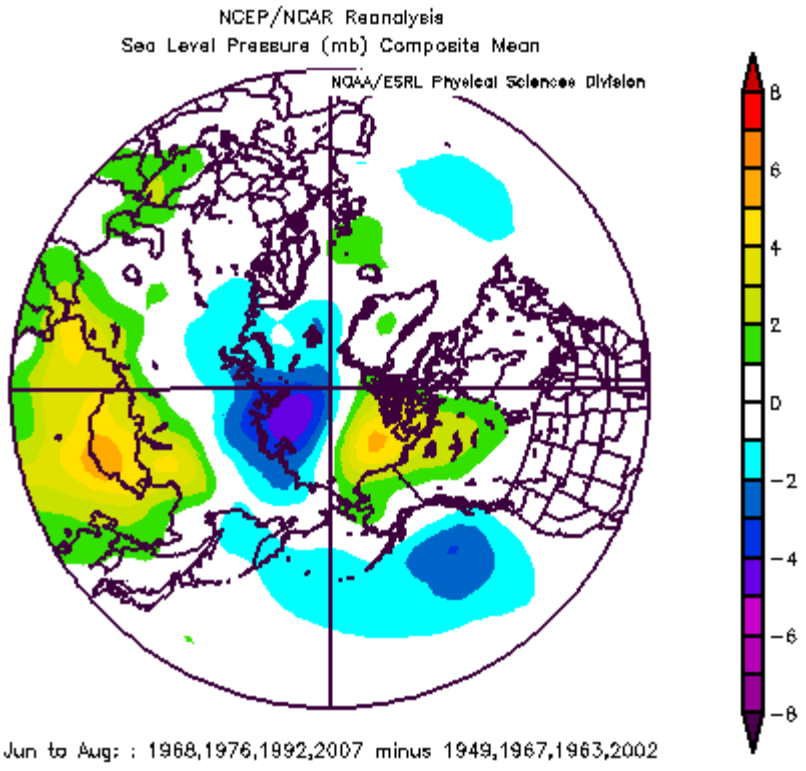

Figure 3.6(c): same as (a) but for summer

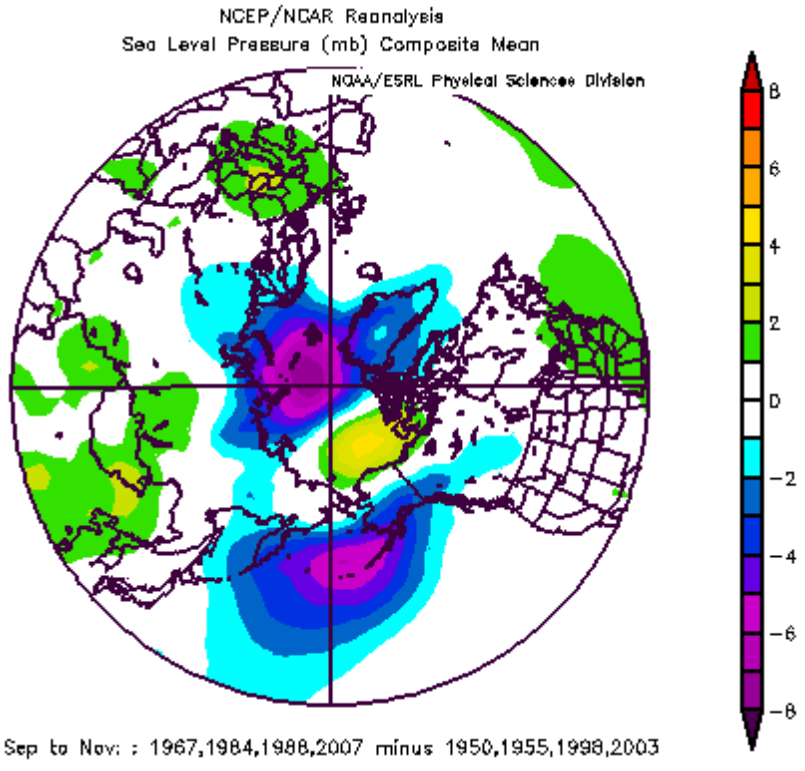

Figure 3.6(d): same as (a) but for autumn

3.2 Temporal Variability

The first timeseries shown earlier in figure 3.5 was used to find seasonal extremes for spatial analysis. In order to characterize the temporal variability and trends of the Beaufort Anticyclone, other timeseries were created and analyzed.

The first timeseries shown in this section is the climatology of the monthly vorticity values for the 1948-2008 time period. Figure 3.7(a) shows the vorticity value for each month. These values were also used in section 3.1 to remove the annual cycle from figure 3.2. There is a vorticity minimum in June with 3 vorticity maxima in February, August, and November. Figure 3.7(b) shows the monthly climatology using averaged SLP; this figure shows the same results as Serreze and Barrett, 2010, with pressure maxima in March and April and minimum in August. The differences between figure 3.7(a) and (b) findings may be attributed to vorticity's capturing of changes in pressure gradients. It is not surprising the vorticity climatology shows differing results from the SLP climatology. As seen earlier in section 3.1, SLP correlations show a signal consistent to Walsh 1978 and Cullather and Lynch 2003 and not consistent with the vorticity correlation signal.

The next timeseries (figure 3.8) shown is the monthly areal average of vorticity. The monthly vorticity value over the Beaufort Sea region produces a noisy and highly variable signal. It is difficult to draw conclusions on trends from a timeseries with this much variability. A running mean was performed on the monthly timeseries at the 3, 6, 12, 24, and 60 month lengths to smooth the noise and identify low-frequency variations in the Beaufort Anticyclone. Figure 3.9 shows the 3 and 6 month running mean. These timeseries still show a noisy signal, but figure 3.10, the 12, 24, and 60

months running means, begin to show interesting variations. There appears to be a decrease in vorticity until 1960 when there is an increase until 1969, the following 20 years show a slow decrease in the vorticity value and finally a slow increase to the end of the timeseries. The AO teleconnection has also shown positive values during throughout much of the 1990's; previous studies on the AO show that with positive index values, positive vorticities are expected as well. The correlations with the AO teleconnection index are discussed in detail later in this section. The 60 month running mean shows this signal the smoothest, but it is prevalent in the 12 and 24 month running mean as well.

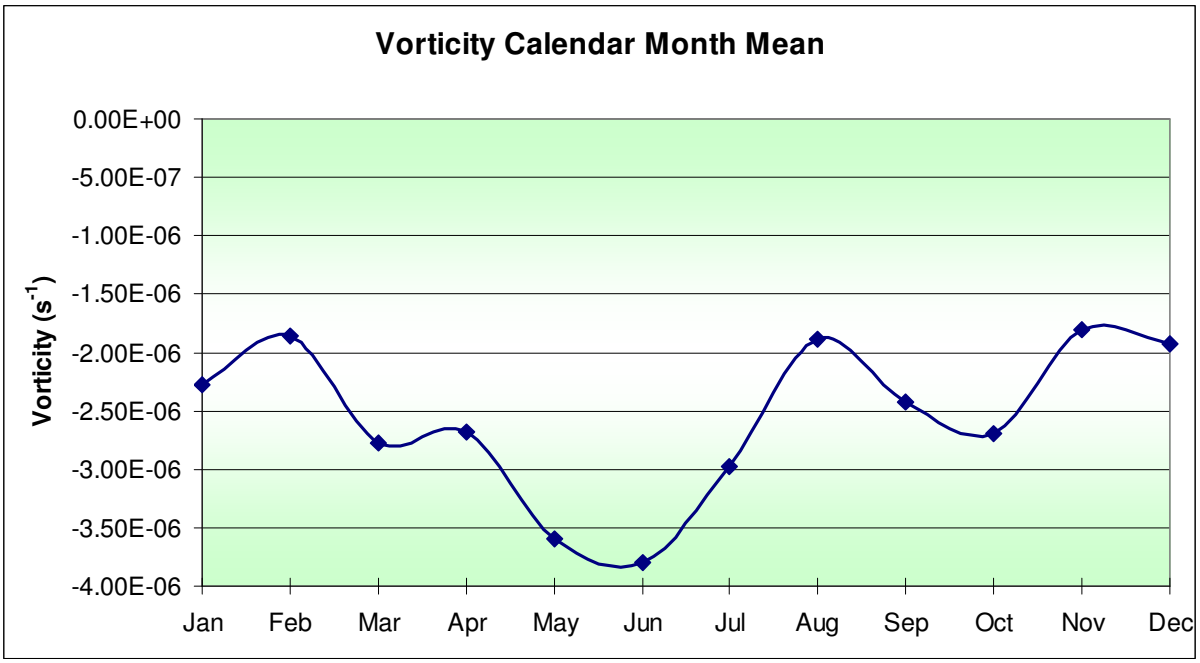

Figure 3.7(a): Monthly climatology for averaged vorticity from 1948-2008

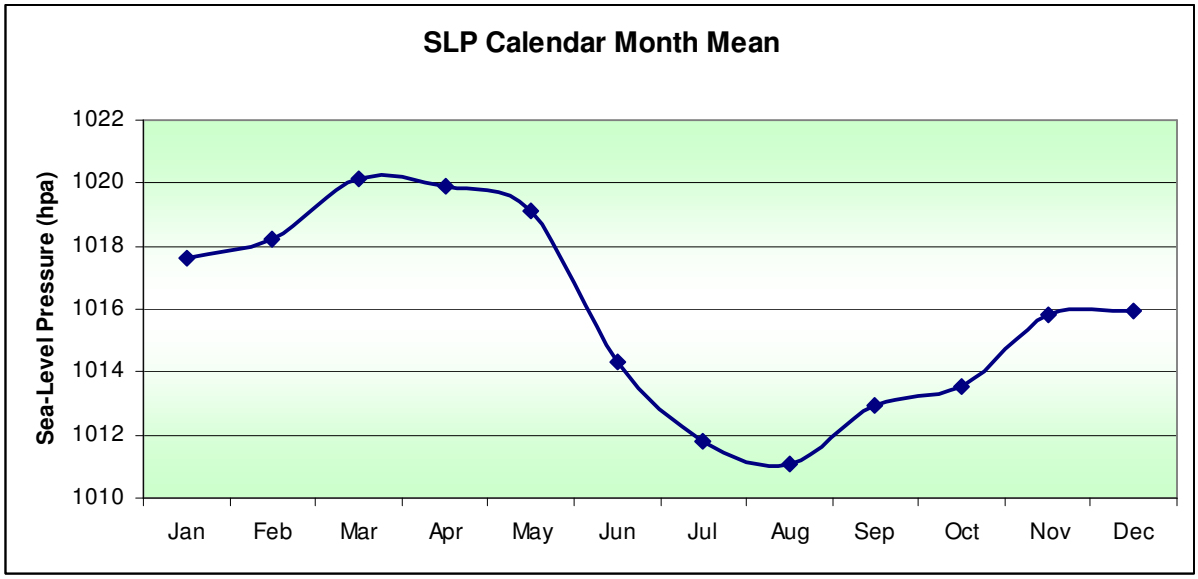

Figure 3.7(b): Monthly climatology for averaged SLP averaged from 1948-2008

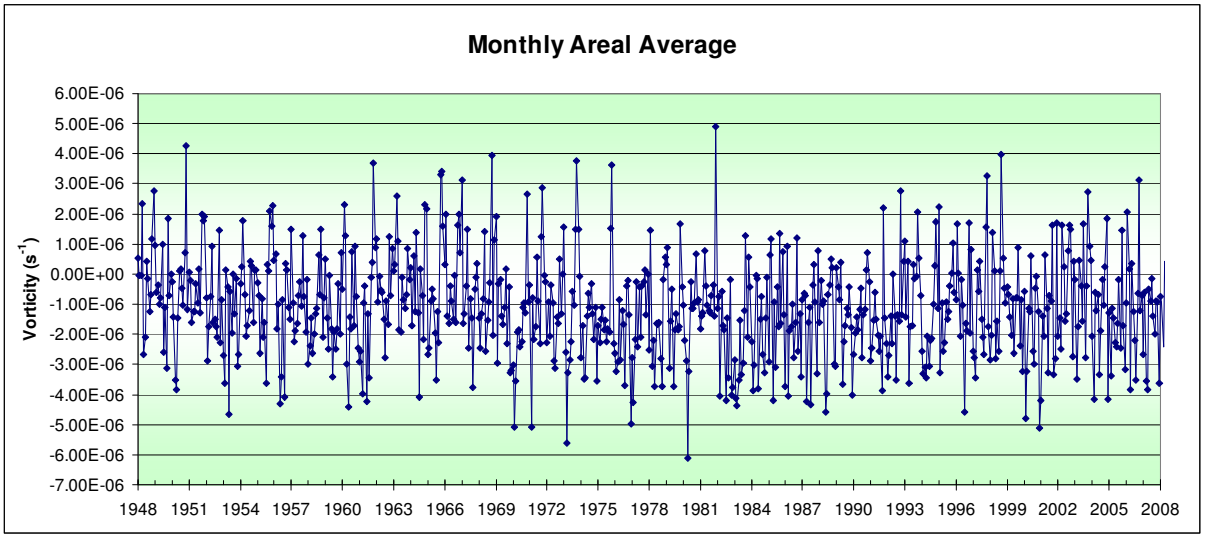

Figure 3.8: Monthly areal average of vorticity

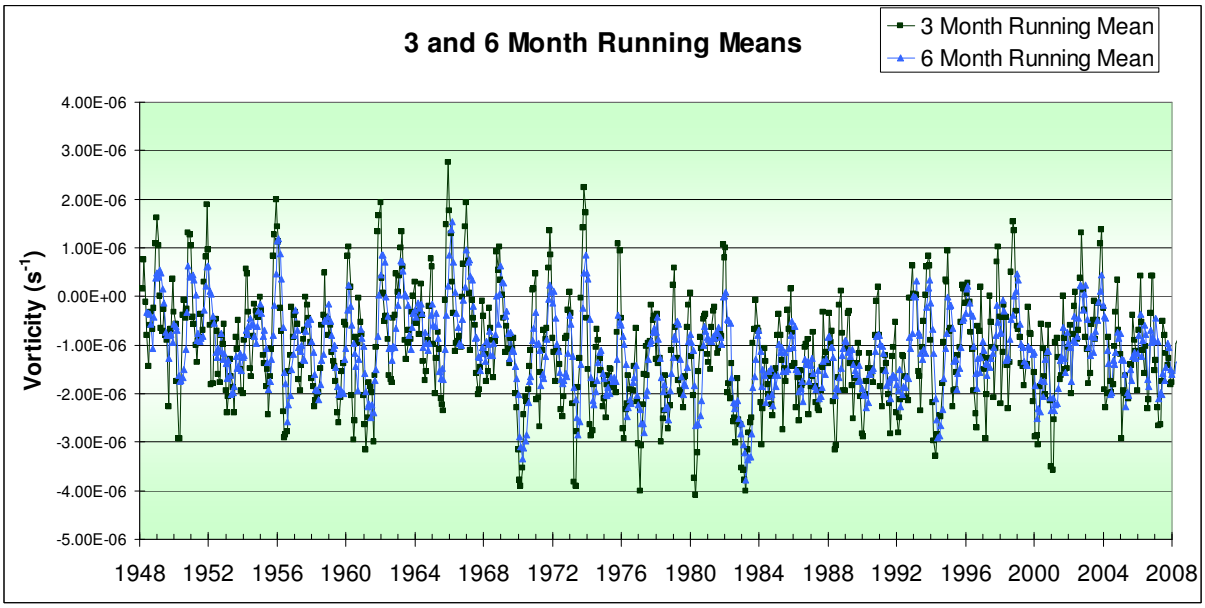

Figure 3.9: 3 and 6 month running mean of monthly areal timeseries

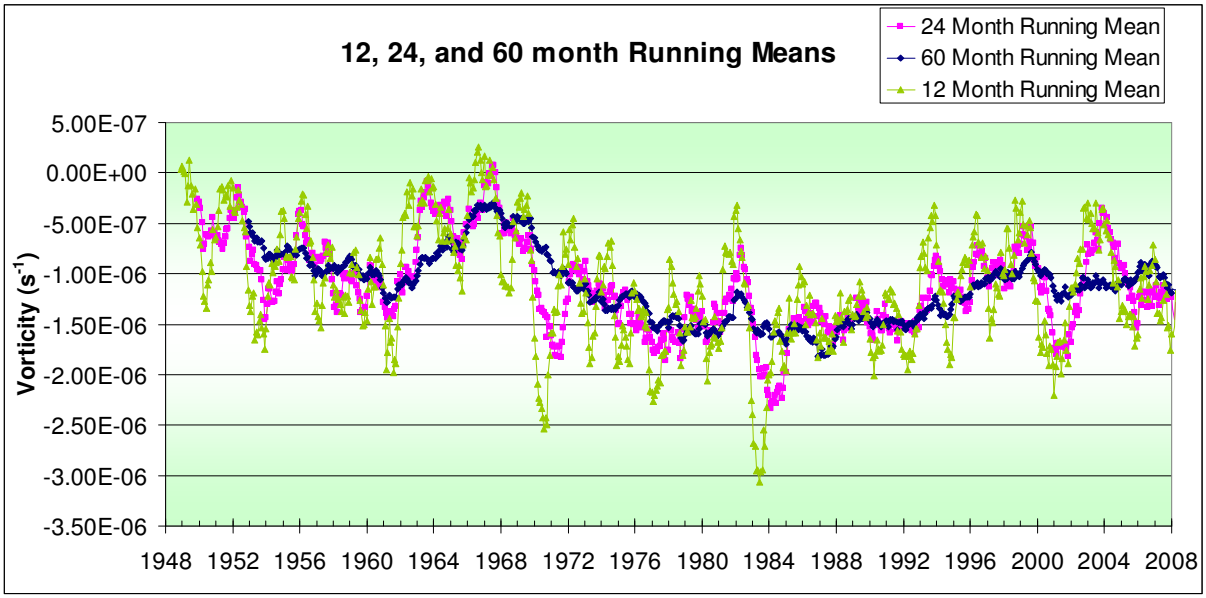

Figure 3.10: 12, 24, and 60 month running mean of monthly areal average

As stated in section 1, 1949 introduced the IABP bouy program. Figure 3.11 shows a comparison of the 1948-1978 and 1979-2008 periods to the entire 1948-2008 climatology. The means for the time periods are relatively similar with the exception of October, November, and December. If those three months are looked at separately as in figure 3.12, the regression lines for the early time period versus the late time period may hold the answer. The 1948-1978 period mean value is greater than the 1979-2008 mean value. This would indicate a strengthening of the Beaufort Anticyclone vorticity in the later period on the average for those three months. The reasons for this strengthening are unknown and need to be investigated further. There are implications for faster sea ice movement and stronger ocean currents if the Beaufort Anticyclone is strengthening. As seen in past studies, L'Heureux et. al, 2008, a stronger Beaufort Anticyclone leads to larger sea ice retreat, and if the Beaufort Anticyclone is indeed strengthening during the autumn months, there may be an increase in sea ice retreat in the future. This is another area that needs further investigation.

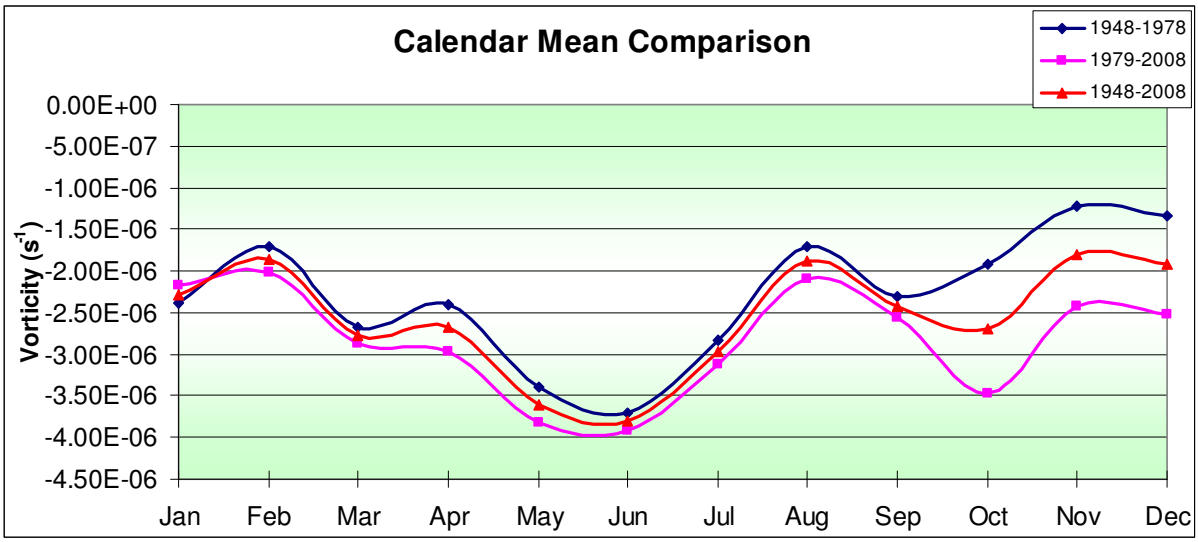

Figure 3.11: A comparison of the 1948-1978 and 1979-2008 averaged calendar mean values

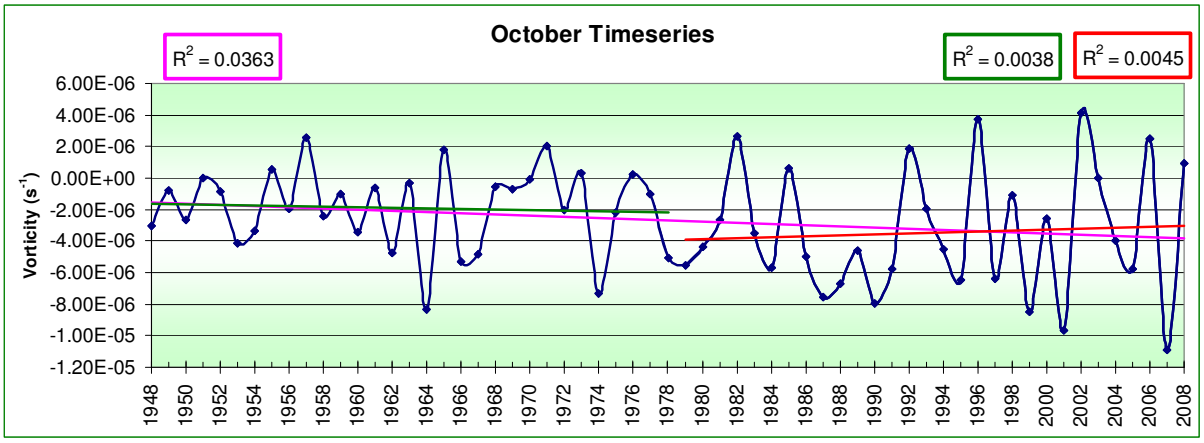

Figure 3.12(a): Monthly timeseries for October with linear regression lines for the 1948-1978 (green), 1979-2008 (red), and 1948-2008 (pink) time periods

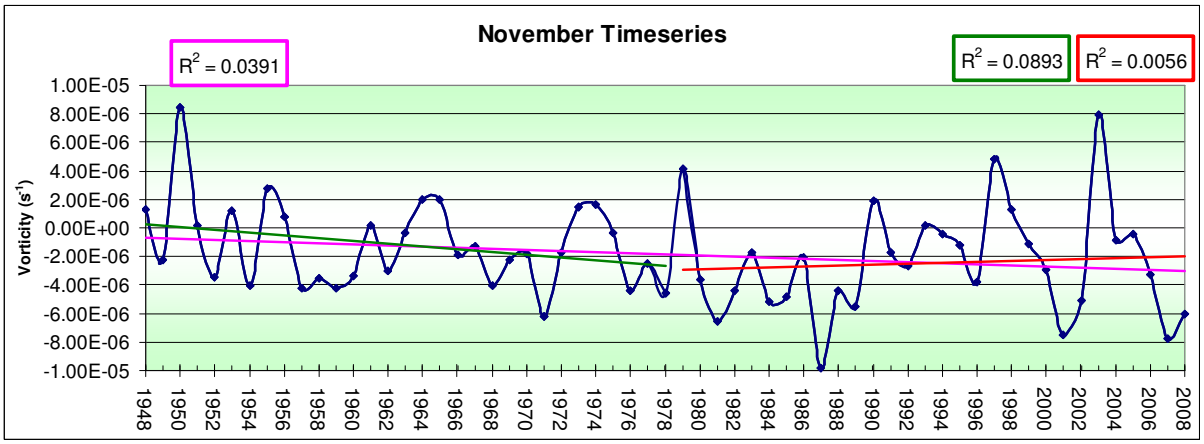

Figure 3.12(b): Same as (a) but for November

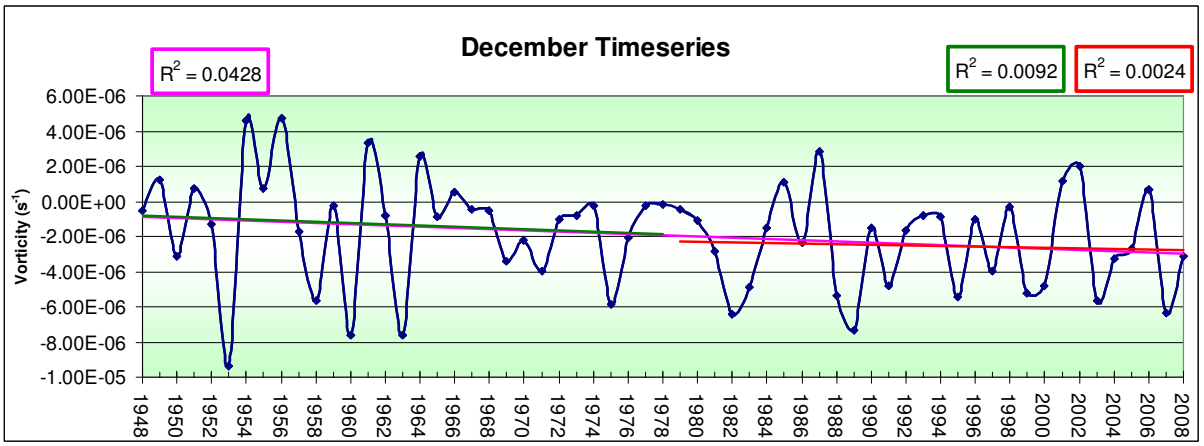

Figure 3.12(c): Same as (a) but for December

3.2.1 Spectral Analysis

Spectral analysis uses Fourier decomposition to locate any periodic signals within a timeseries. The monthly and running mean timeseries were sent through the spectral analysis code downloaded from http://mahi.ucsd.edu/cathy/Classes/SIO223/SIO223.html to locate any periodic signals within the Beaufort Anticyclone. Figure 3.13 shows the results of spectral analysis on the monthly timeseries. There is a peak at around .08 cycles per month indicating one complete cycle every 12 months. This shows the Beaufort Anticyclone has an annual cycle. There were no other periodic cycles found, although figure 3.13 does show that there is more variance in lower frequencies than in higher frequencies. The lower frequency variation does provide support to the Proshutinsky and Johnson, 1997, result of an oscillation of 3-5 years between an anticyclonic and cyclonic wind regime over the Arctic Ocean.

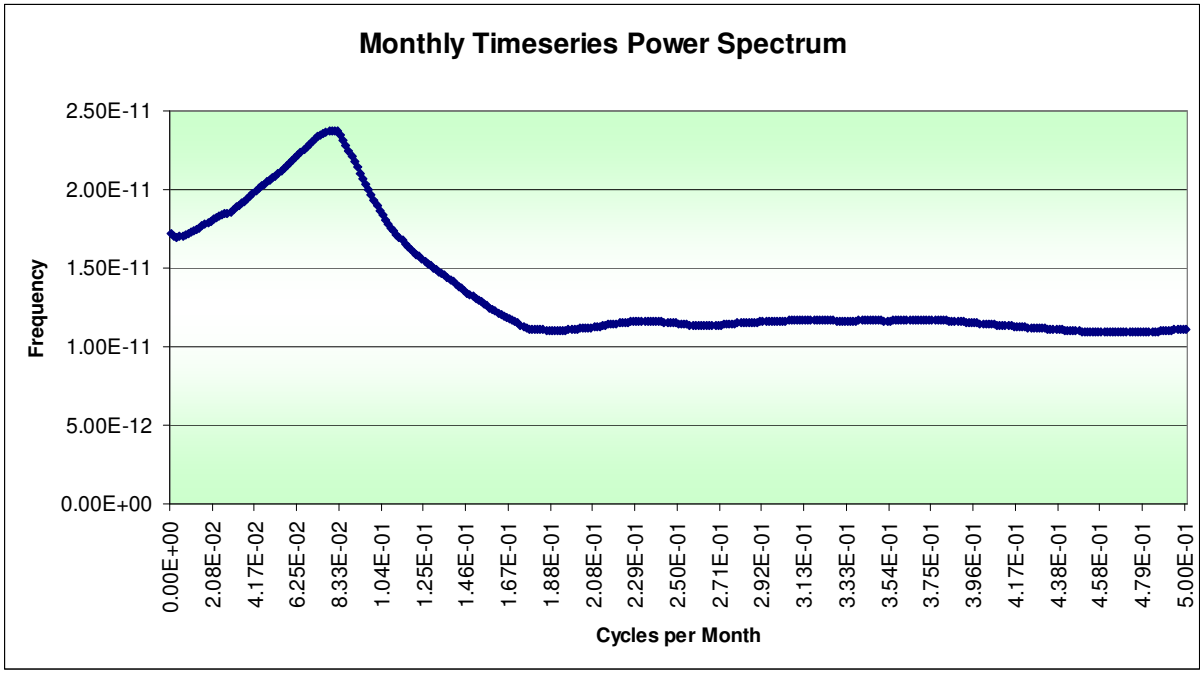

Figure 3.13: Power spectrum of monthly timeseries showing the frequency of cycles per month

3.3 Rapid Change Events

To better understand mass flux associated with the Beaufort Anticyclone, 30-day running mean periods were examined for largest change in vorticity over the Beaufort Sea region. The 30-day running mean was chosen to capture the monthly timescale without the constraint of the 1st/31st beginning and end to the month. Figure 3.14 is a timeseries of the rapid change events calculated by finding the difference between two 30-day running means. The endpoints for the rapid change events are 30 days apart. The most extreme positive and negative rapid change events were identified using this timeseries and then further investigated by creating figures of SLP to identify where regions of increasing and decreasing pressure are located.

Figure 3.15 shows the change in SLP for the most rapid change events for both increasing and decreasing vorticity. These events were chosen by locating the maximum and minimum vorticity changes shown in figure 3.14. Figure 3.15(a) shows the rapid decrease event between September 16, 1957 and October 16, 1957. There appears to be numerous areas of increasing and decreasing SLP extending from the Aleutian Low region across Siberia and into the Northern Atlantic Ocean. The centers of SLP change are located over the Beaufort region, south of Alaska, north of Siberia, south of Finland, and over Great Britain. Figure 3.15(b) shows the rapid increase event between September 22, 1987 and October 22, 1987. This rapid change event shows areas of increasing and decreasing SLP in the same locations as figure 3.15(a), but generally with opposite sign. This result provides an interesting hypothesis that there are areas of SLP change over the Beaufort region, south of Alaska, north of Siberia, south of Finland, and over Great Britain of during one of these rapid change events. In

order to investigate this further, composite figures of the 5 and 10 most extreme events were created.

If the 5 most extreme rapid change events are composited, as shown in figure 3.16, the signal found in figure 3.15 remains robust. Figures 3.16 (a) and (b) do not show strong signals for all the centers outlined in figure 3.15, but the composite difference shown in figure 3.16 (c) shows all centers of action in similar locations as figure 3.15. Further, the Aleutian and Siberian centers of action are generally the same regions that showed a stronger correlation to the Beaufort Anticyclone in figure 3.2. This is an expected result that further confirms the hypothesis that these regions are important for mass flux over the Beaufort region. This pattern remains robust if the 10 most extreme events are composited as shown in figure 3.17.

A dynamical interpretation of the pattern of SLP change during the rapid change events is an area that will require future investigation.

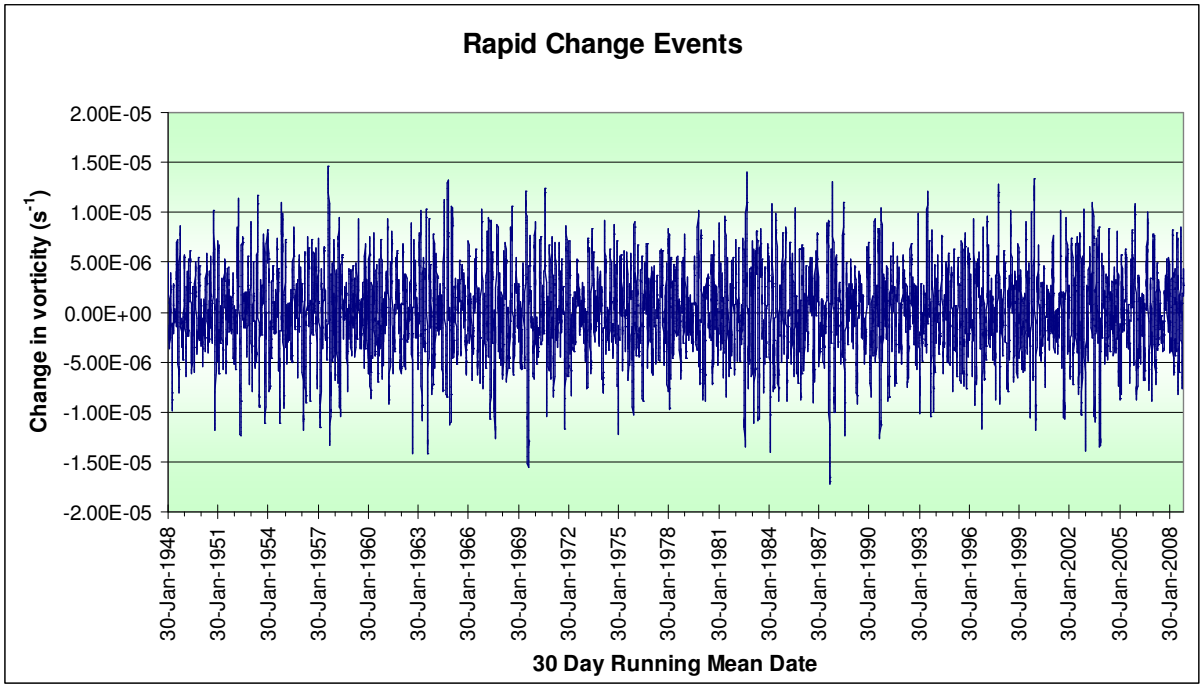

Figure 3.14: Timeseries of rapid change events. Running mean date refers to the end of the rapid change event.

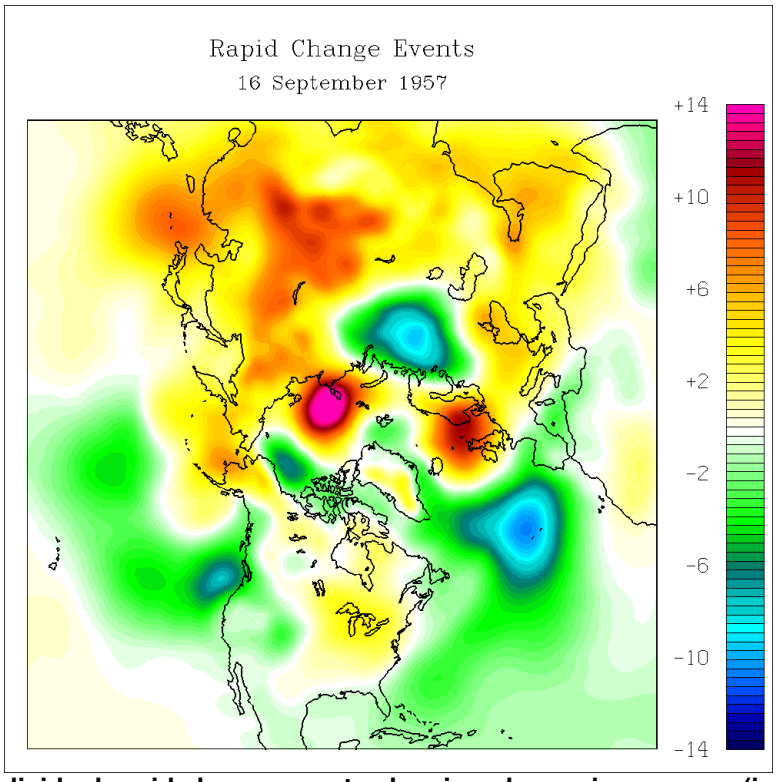

Figure 3.15(a): Individual rapid change events showing change in pressure (in hpa). Most rapid decrease event from figure 3.13

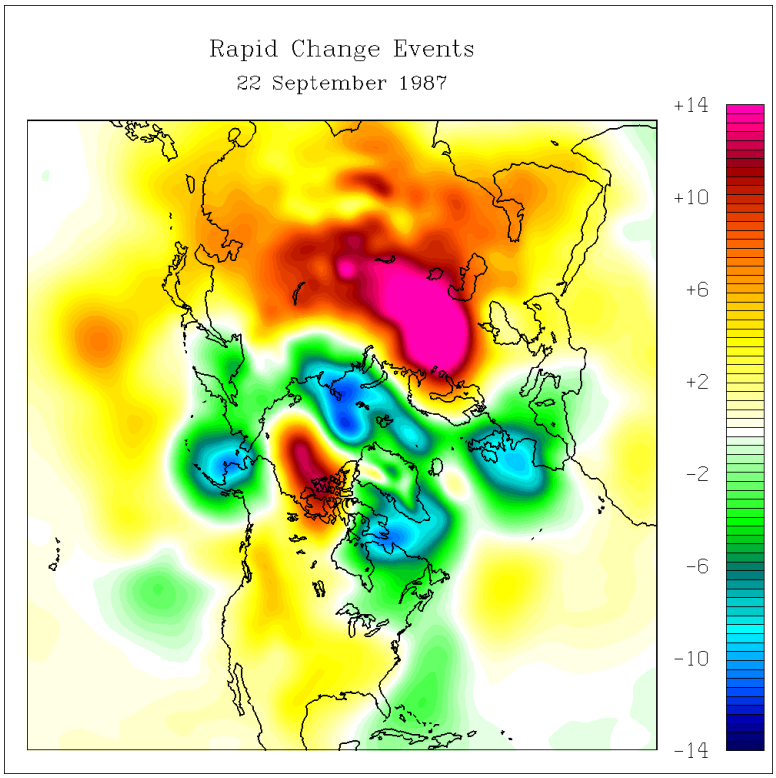

Figure 3.15(b): Same as (a) but for the most rapid increase event

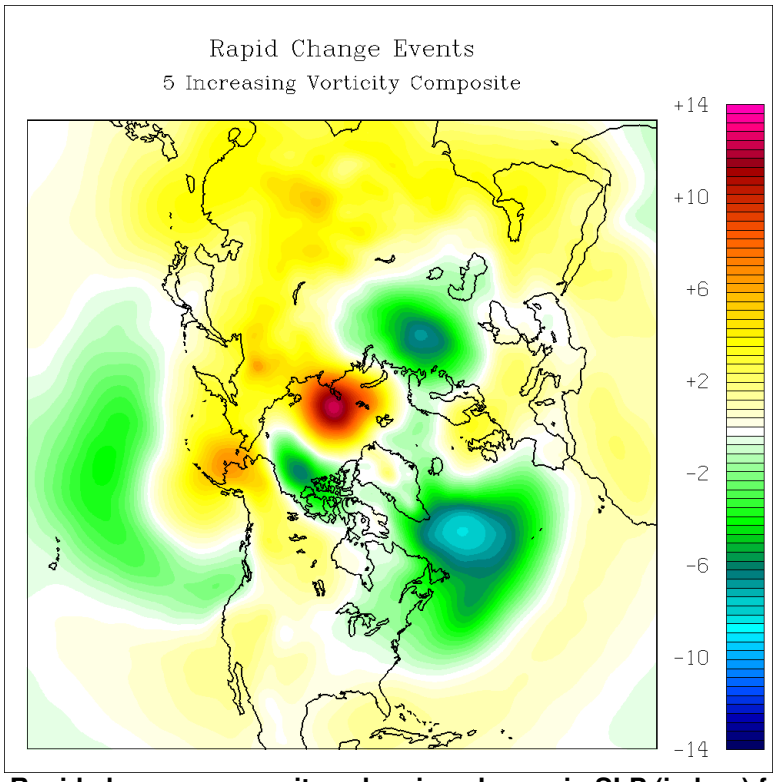

Figure 3.16(a): Rapid change composites showing change in SLP (in hpa) for 5 increasing vorticity events using figure 3.13

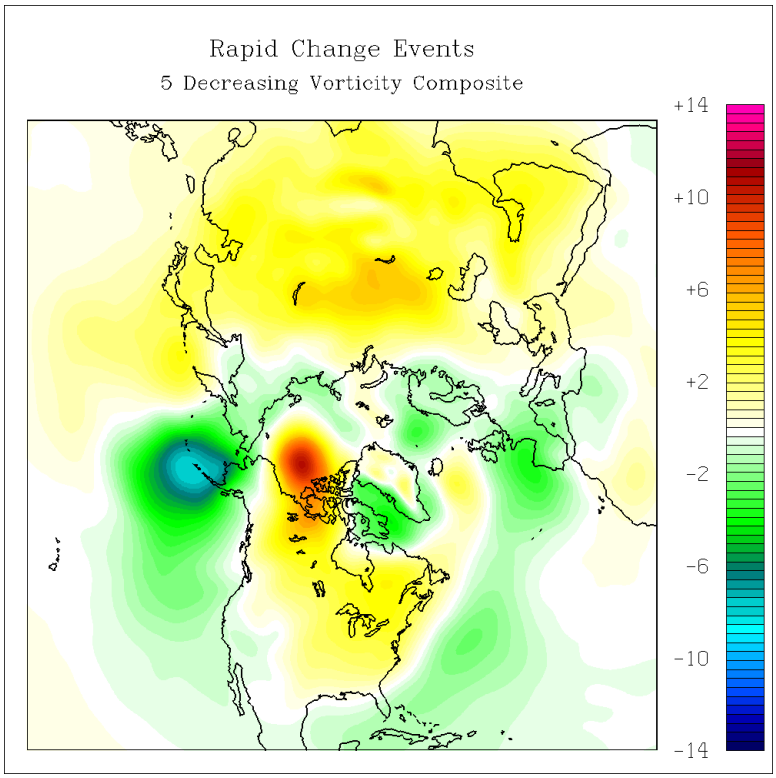

Figure 3.16(b): same as (a) but for 5 decreasing vorticity events

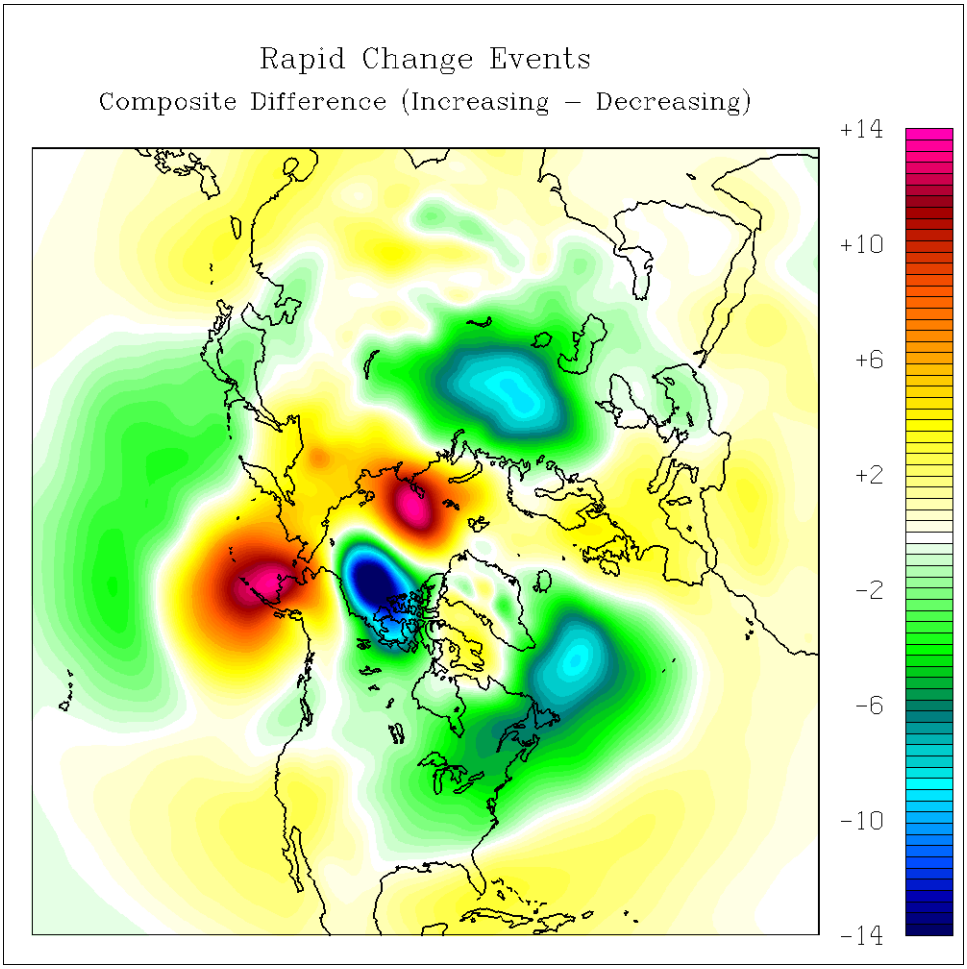

Figure 3.16(c): Composite difference field found by subtracting (a) – (b)

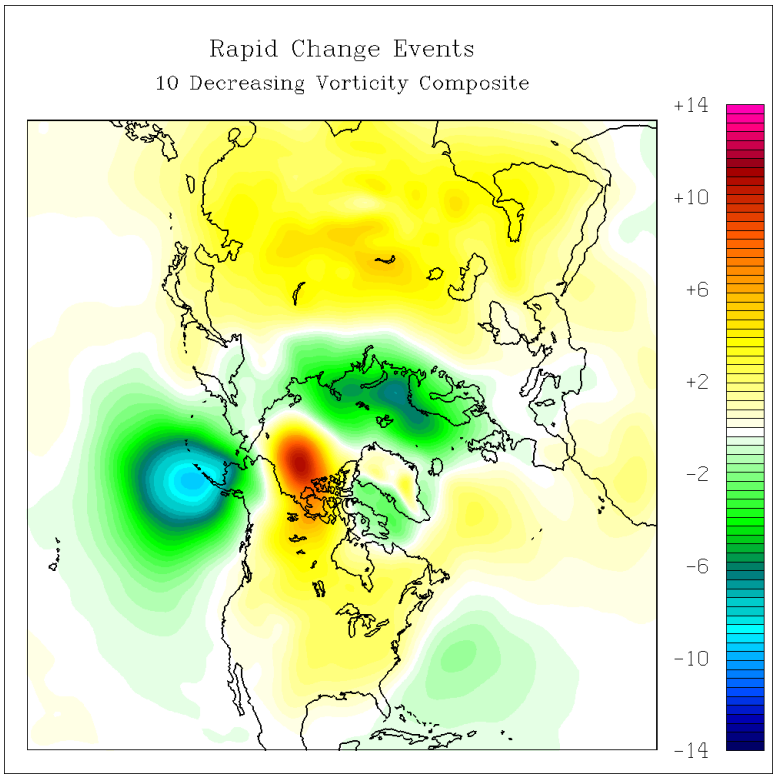

Figure 3.17(a): Rapid change composites (in hpa) for 10 increasing vorticity events using figure 3.13

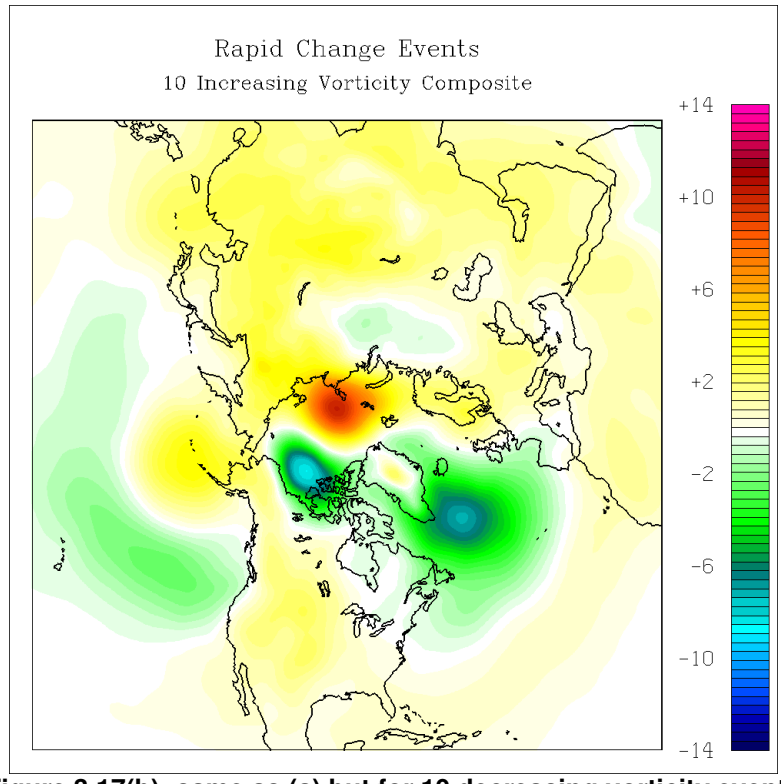

Figure 3.17(b): same as (a) but for 10 decreasing vorticity events

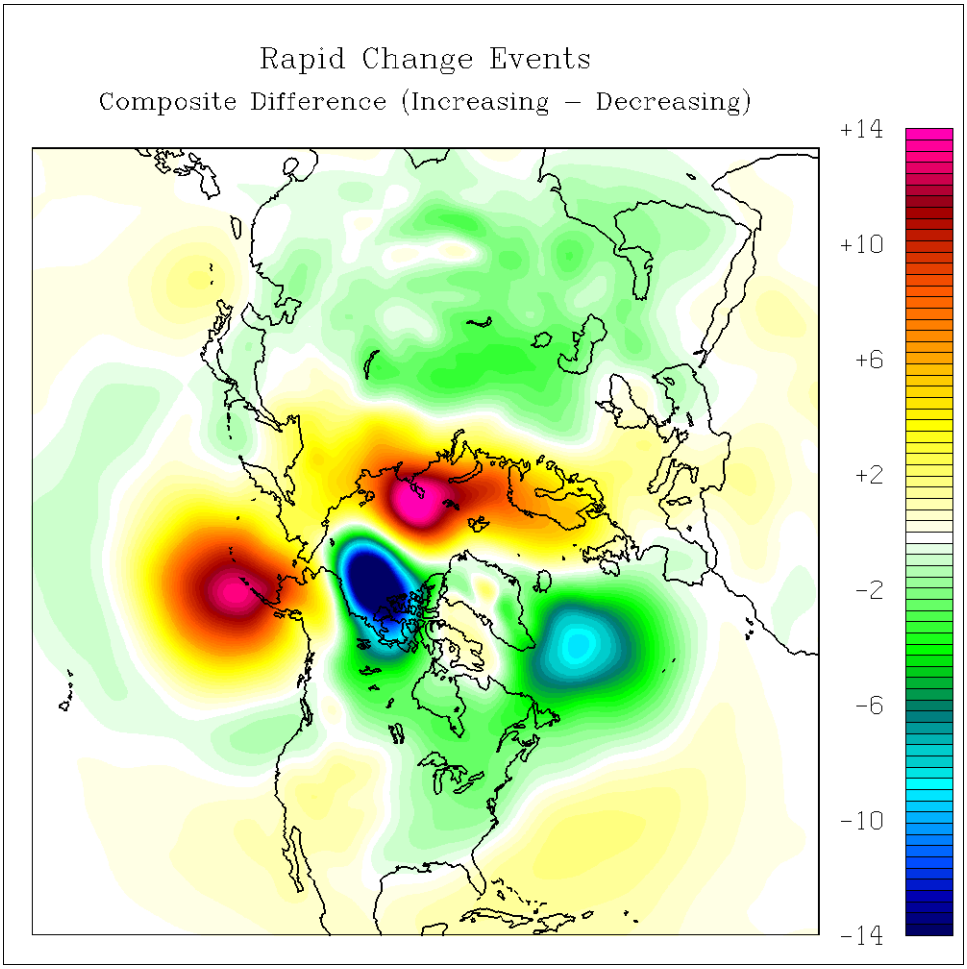

Figure 3.17(c): Composite difference field found by subtracting (a) – (b)

3.4 Teleconnection influences on the Beaufort Anticyclone

If the teleconnection maps shown in section 2 are examined, it becomes apparent that some have centers of action located in the Arctic. The AO is the main teleconnection thought to influence the pressure patterns over the Arctic. As discussed earlier, there are main centers of action in the AO over the Northern Pacific, Northern Atlantic, and Arctic Oceans. However, in comparing the AO signature to the vorticity correlations in figure 3.2, there does not appear to be much similarity in pattern, but SLP index does show the AO in its correlations with SLP as shown in figure 3.4. The correlation center south of Alaska is consistent with the AO signature over the North Pacific; however, the other centers of action are not present. This is also true for the NAO pattern which has centers of action over the North Atlantic and Greenland areas, not over the Beaufort or correlation regions. The ENSO teleconnection pattern also shows no similarity to the correlation pattern, but this is not surprising since the ENSO pattern mainly affects the tropical Pacific. The two teleconnection patterns that show any similarities are the PNA and PDO patterns. Both have main centers of action south of Alaska, in the same location as the correlation center. It is therefore important to investigate which teleconnection patterns may have a role in the variability of the Beaufort Anticyclone.

To investigate the Beaufort Anticyclone's interactions with the teleconnection patterns outlined in section 2, each teleconnection index is correlated with the averaged vorticity value over the Beaufort region. The results are shown in figure 3.18. The largest correlation is found with the PNA pattern in all seasons. This result is consistent with L'Heureux et. al, 2008 study showing the correlation between the PNA

and the Beaufort region to be significant. It should also be noted that the patterns in the Pacific Ocean show higher correlation values than the Atlantic Ocean. Also, the ENSO pattern shows a relatively large correlation signal in winter, which implies some tropical connection to the Beaufort Anticyclone. This implication is supported by the correlations found with areas of significance in figures 3.2 and 3.3 Using a basic significance test of $(2/\sqrt{n})$, correlation values in figure 3.18 were found to be significant if greater than 0.26 or less than -0.26 as shown by the darkened line on figure 3.18.

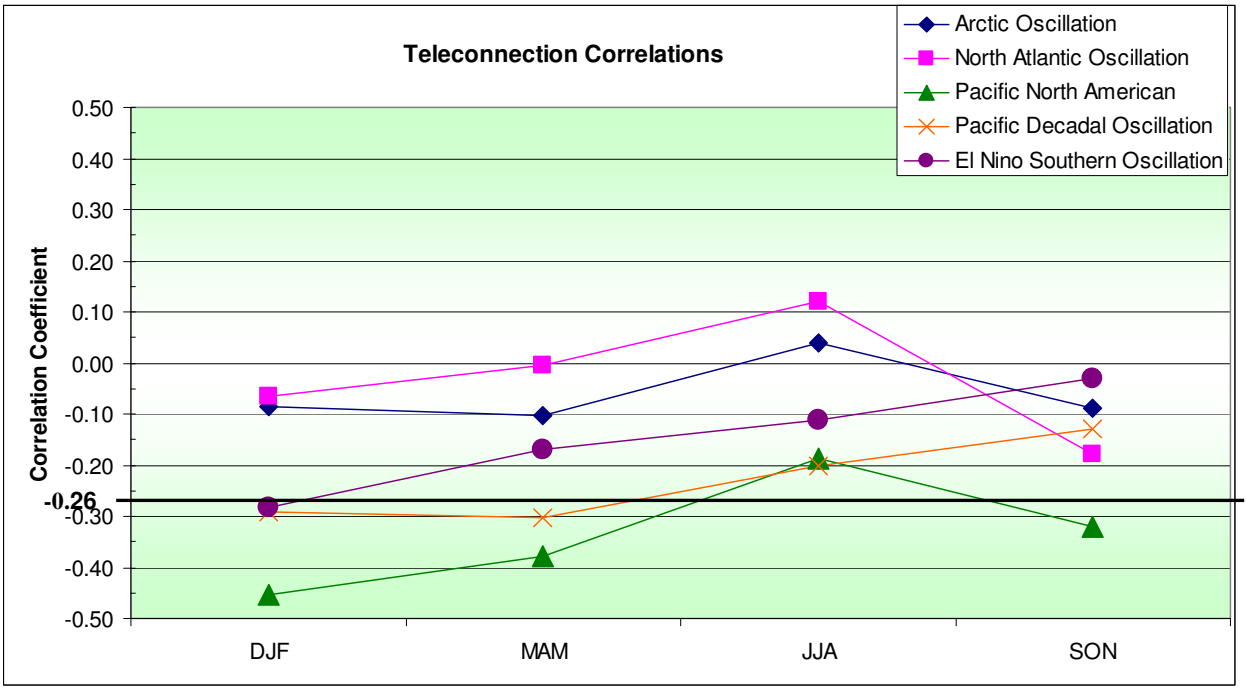

Figure 3.18: Teleconnection index values correlated with the Beaufort vorticity metric.

4. Conclusions

4.1 Summary of Results

The use of a vorticity metric to investigate the Beaufort Anticyclone has provided new insight into the dynamic Arctic System. Previous studies have hypothesized that the Beaufort Anticyclone builds and decays as mass is transported between the Atlantic and Pacific Oceans (Cullather and Lynch, 2003). This see-saw pattern is found in the SLP correlations but not in the vorticity correlations. Vorticity correlations show centers of action south of Alaska and north of Siberia not found in the SLP correlations. These areas are also prevalent in SLP composites and rapid vorticity change events. Leading to the conclusion that vorticity is capturing a signal based on changes in the Beaufort Anticyclone's pressure gradient by changing either the magnitude or location of the anticyclone.

Analysis of the climatology of the Beaufort Anticyclone shows the minimum vorticity in June with the maximum SLP in March and April. The difference in month is likely due to a stronger pressure gradient over the Beaufort region in June due to vorticity's sensitivity to changes in the pressure gradient.

Further temporal analysis of running means show a slow increase in recent years of Beaufort vorticity magnitude. This result has strong implications for the pressure over the Beaufort, which in turn has an implication for the wind regime and thus sea-ice movement over the Arctic. In 2007, the Beaufort Anticyclone's vorticity was large, creating large wind speed gradients, and anomalous sea-ice motion and loss over the Arctic. The final temporal investigation method uses spectral analysis on

the Beaufort Anticyclone timeseries. The results show an annual cycle as the only periodic cycle present.

Atmospheric teleconnection patterns have a significant association with the Beaufort Anticyclone. Pacific teleconnection patterns were shown to have more significant interactions than Atlantic patterns. This result is contrary to past studies that indicate the Arctic Oscillation as a major driver of pressure over the Arctic. It is possible the results reflect the hypothesis that the vorticity metric is capturing a smaller scale mass flux pattern. Two of the Pacific Ocean teleconnections that show significance were the PNA and PDO. These have centers of action south of Alaska, similar to the vorticity correlations, creating a region of interaction between these teleconnection patterns and the Beaufort Anticyclone. ENSO also showed significance in winter possibly due to small interactions between the PNA, PDO and ENSO signals. The PNA pattern shows highest correlation, which is consistent with past PNA teleconnection studies (L'Heureux et. al, 2008).

4.2 Future Work

Further investigation of the Beaufort Anticyclone should begin with model simulations of the vorticity metric sensitivity. A model investigation would also allow a study of the interactions of the small scale features documented in this study to the larger scale see-saw mass flux documented in past studies. The exact influences of teleconnections could also be investigated during a model study. A better understanding of the teleconnection interactions with the Beaufort Anticyclone could lead to easier forecasting of the anticyclone’s magnitude and sea-ice motion.

In order to completely understand the Beaufort Anticyclone's NH influences, an investigation of upper level vorticity signatures and correlations should be performed. There are no indications of a Beaufort Anticyclone in the upper troposphere, but any upper level ridge/trough features caused by the Beaufort Anticyclone would be important for mid-latitude storm development. It would also be beneficial to investigate other atmospheric variables over the Beaufort Anticyclone, particularity wind speed and temperature, since those variables have a large influence on sea-ice.

With further investigations, the Beaufort Anticyclone's influence on the Arctic and global systems can be completely understood, providing limitless insight into forecasting a rapidly changing ecosystem.

5. References

Barnston A. G., and R. E. Livezey, 1987: Classification, seasonality and persistence of low-frequency atmospheric circulation patterns. *Mon. Wea. Rev.*, **115**, 1083-1126.

Climate Prediction Center, cited 2010: AO, NAO, PNA Index. [Available online at http://www.cpc.noaa.gov/products/precip/CWlink/daily_ao_index/teleconnections.shtml]

Coon, M. D., G. A. Maykut, R. S. Pritchard, D. A. Rothrock and A. S. Thorndike, 1974: Modeling the pack ice as an elastic-plastic material. *AIDJEX Bull.,* **24**, 1-105

Crutcher, H. L., and J. M. Meserve, 1970: Selected level heights, temperature, and dew points for the northern hemisphere. *NAVAIR 50-IC-52 rev.*, Naval Weather Service Command, Washington DC.

Cullather, R. I. and A. H. Lynch, 2003: The annual cycle and interannual variability of atmospheric pressure in the vicinity of the North Pole. *International J. of Climatology*, **23**(10), 1161-1183.

Honda M, Nakamura H, Ukita J, Kousaka I, Takeuchi K. 2001: Interannual seesaw between the Aleutian and Icelandic lows part I: seasonal dependence and life cycle*. J. Climate,* **14,** 1029-1042

International Arctic Buoy Programme, cited 2010. [Available online at http://iabp.apl.washington.edu/index.html]

Kalnay, E. and et al., 1996: The NCEP/NCAR Reanalysis 40-year project*. Bull. Amer. Meteor. Soc.*, **77**, 437-471.

Kistler, R., and Coauthors, 2001: The NCEP–NCAR 50-year reanalysis: Monthly means CD-ROM and documentation. *Bull. Amer. Meteor. Soc.,* **82,** 247–267.

L'Heureux M. L., A. Kumar, G. D. Bell, M. S. Halpert, R. W. Higgins, 2008: Role of the Pacific-North American (PNA) pattern in the 2007 Arctic sea ice decline, *Geophys. Res. Lett.*, **35**, L20701, doi:10.1029/2008GL035205.

Lutengs F.K and E.J. Tarbuck 2001: *The Atmosphere.* Prentice Hall, 8th ed. Figure 7.7

Mantua, N.J., cited 2010: PDO Index. [Available online at http://jisao.washington.edu/pdo/.]

Mesquita M. S., D. E. Atkinson, K. I. Hodges, 2010: Characteristics and variability of storm tracks in the North Pacific, Bering Sea, and Alaska, *J. Climate.,* **23:2**, 294-311

O'Connor, J. F. 1961: Mean circulation patterns based on 12 years of northern hemisphere data. *Mon. Wea. Rev.,* **89**, 211-227.

Ogi, M., I.G. Rigor, M.G. McPhee, and J.M. Wallace, 2008: Summer retreat of Arctic sea ice: Role of summer winds. *Geophys. Res. Lett.*, **35**, L24701, doi: 10.1029/2008GL035672,

Ogi, M., K. Yamazaki, and J. M. Wallace, 2010, Influence of winter and summer surface wind anomalies on summer Arctic sea ice extent, *Geophys. Res. Lett.*, **37**, L07701, doi:10.1029/2009GL042356.

Petterssen S. 1969: *Introduction to Meteorology*. McGraw-Hill Inc. 3rd ed. 416pp.

Prik, Z. M., 1959: Mean position of the surface pressure and temperature distribution in the Arctic. *Tr. Arktic. Nauch. Issled. Inst.,* **217,** 5-34

Proshutinsky, A.Y., and M.A. Johnson, 1997: Two circulation regimes of the wind-driven Arctic Ocean. *J. Geophys. Res.*, **102(C6)**, 12493-12514, doi:10.1029/97JC00738

Rayner, N.A., Parker, D.E., Horton, E.B, Folland, C.K., Alexander, L.V., Rowell, D.P., Kent, E.C., Kaplan, A., 2006: UKMO - GISST/MOHMATN4/MOHSST6 - Global Ice coverage and SST (1856-2006), [Internet]. UK Meteorological Office

Reed, R. J., and B. A. Kunkel, 1960: The Arctic circulation in summer. *J. Meteor.*, **17,** 489-506.

Reynolds, R. W., 1988: A real-time global sea surface temperature analysis. *J. Climate*, **1**, 75-86.

Rigor, I.G., J.M. Wallace, and R.L. Colony, 2002: Response of sea ice to the Arctic Oscillation. *J. Climate,* **15**, 2648-2663.

Serreze, M. C., Barry R. G., 1988: Synoptic activity in the Arctic Basin, 1979-85. *J. Climate*, **1**(12), 1276-1295

Serreze, M. C., J. E. Box, R. G. Barry, J. E. Walsh, 1993: Characteristic of Arctic synoptic activity, 1952-1989. *Meteorol. Atmos. Phys.* **51,** 147-164.

Serreze, M. C. and A. P. Barrett, 2010: Characteristics of the Beaufort Sea High. *Submitted to J. Climate*

Smith, C.A. and P. Sardeshmukh, 2000: The effect of ENSO on the intraseasonal variance of surface temperature in winter., *International J. of Climatology*, **20** 1543-1557.

Thorndike, A. S. and R. Colony, 1980: *Arctic Ocean Buoy Program Data Report, 1 January 1979-31 December 1979*. Polar Science Center, University of Washington, Seattle, 131 pp.

Wallace, J.M., and D.S. Gutzler, 1981: Teleconnections in the geopotential height field during the Northern Hemisphere winter. *Mon. Wea. Rev.*, **109**, 784-812.

Wallace, J. M., and P. V. Hobbs, 2006: *Atmospheric Science: An Introductory Survey*. Academic Press, 2nd ed. 350 pp.

Walsh, J.E., 1978: Temporal and spatial scales of the Arctic circulation. *Mon. Wea. Rev.*, **106**, 1532–1544.

Wang, J., J. Zhang, E. Watanabe, M. Ikeda, K. Mizobata, J.E. Walsh, X. Bai, and B. Wu, 2009: Is the dipole anomaly a major driver to record lows in Arctic summer sea ice extent. *Geophys. Res. Lett.*, **36**, L05706, doi:10.1029/2008GL036706